The Anatomy of the Pion Loop Hadronic Light by Light Scattering Contribution to the Muon Magnetic Anomaly

Mehran Zahiri Abyaneh

Thesis advisor: Johan Bijnens

Department of Theoretical Physics, Lund University

Sölvegatan 14A, S22362 Lund, Sweden

Abstract

This thesis investigates the Hadronic Light by Light (HLL) scattering contribution to the muon $g - 2$, which is one of the most important low energy hadronic effects and consists mainly of the quark loop, the pion pole and the charged pion and kaon loops. In this work the charged pion loop has been investigated more closely. After reviewing the subject a preliminary introduction to Chiral Perturbation Theory (ChPT), Hidden Local Symmetry (HLS) model and the full Vector Meson Dominance (VMD) model is given, and they are used to calculate the pion loop HLL scattering contribution to the muon anomalous magnetic moment. The momentum regions where the contributions of the bare pion loop, the VMD model, and the HLS come from, have been studied, to understand why different models give very different results. The effects of pion polarizability and charge radius on the HLL scattering, which appear at order p^4 in ChPT, from L_9 and L_{10} Lagrangian terms and their momentum regions have been studied.

Master of Science Thesis

Contents

1 Introduction

1.1 Theory

Elementary particles have some inherent properties including charge, mass, spin and life-time. As important as these quantities, are the magnetic and electric dipole moments which are typical for charged particles with spin. Classically, an orbiting particle with electric charge e carrying mass m entails a magnetic dipole moment given by

$$\boldsymbol{\mu} = \frac{e}{2m}\mathbf{L} \ , \tag{1.1}$$

where $\boldsymbol{L}$ is the angular momentum of the particle. Magnetic and electric moments interact with external magnetic and electric fields via the Hamiltonian

$$H = -\boldsymbol{\mu} \cdot \mathbf{B} - \mathbf{d} \cdot \mathbf{E} \ , \tag{1.2}$$

where $\mathbf{B}$ and $\mathbf{E}$ are the magnetic and electric field strengths and $\boldsymbol{\mu}$ and $\mathbf{d}$ the magnetic and electric dipole moment operators. The magnetic moment is often measured in units of the Bohr magneton $\boldsymbol{\mu}_B$ which is defined as

$$\mu_B = \frac{e}{2m_e} = 5.788381804(39) \times 10^{-11} \text{MeVT}^{-1} \ , \tag{1.3}$$

where T stands for Tesla. When it comes to spinning particles, the angular momentum operator in (1.1) should be replaced by the spin operator [1].

For a charged elementary particle with intrinsic spin and charge q, the magnetic moment is written

$$\boldsymbol{\mu} = g_s \frac{q}{2m}\mathbf{S} \ , \tag{1.4}$$

where, $\mathbf{S}$ is the spin operator. The constant g_s is the Lande g-factor. Although the Dirac equation predicts that $g_s = 2$ for electron-like particles, it is slightly greater than 2, and theoretically it is useful to break the magnetic moment into two pieces

$$\mu = (1 + a)\frac{q\hbar}{m} \ , \tag{1.5}$$

where $a = \frac{g-2}{2}$. The first piece, called the Dirac moment, is 2 in units of the Bohr magnetic moment. The second piece is called the anomalous (Pauli) moment, and a is a dimensionless quantity referred to as the anomaly.

In 1947, Schwinger, having managed to eliminate divergencies arising in the calculation in loop corrections in QED, showed that the deviation of g_s from 2 can be ascribed to radiative corrections. The first order correction known as the one-loop correction to g = 2, is shown diagrammatically in Figure 1. More generally, the Standard-Model corrections to the electron, muon or tau anomaly, $a(SM)$, arise from virtual leptons, hadrons, gauge bosons and the Higgs boson. This includes the dominant QED terms, which contain only leptons and photons; terms which involve hadrons including hadronic vacuum polarization

2

Figure 1: The Feynman graphs for: (a) g = 2; (b) the lowest-order radiative correction first calculated by Schwinger. Figure from [2].

and hadronic light by light (HLL) corrections, and electroweak terms, which contain the Higgs, W and Z. That is, the anomaly for lepton l is calculated as

$$a_l = a_l^{QED} + a_l^{Had} + a_l^{Weak} \quad . \tag{1.6}$$

An introduction to the theory can be found in [3]. It should be mentioned that, in the Standard Model calculations of a_l, all contributions coming from the mass scale $m_l \gg M$ in loops are suppressed by powers of m_l/M, and all with in the range $M \gg m_l$ are enhanced by powers of $ln(m_l/M)$. Therefore, for the electron, the most important parts come from the QED part where the mediator is the massless photon [1] and the sensitivity to hadronic and weak effects as well as the sensitivity to physics beyond the SM is very small. Typical Feynman diagrams which contribute to the electron magnetic anomaly are shown in Figure 2. This allows for a very precise and model independent prediction of a_e and hence to determine the fine structure constant α with the highest accuracy, which is needed as an input to be able to make precise predictions for other observables like a_μ. This could be done, matching the predicted value of a_e^{SM} [3]

$$a_e^{SM} = 0.5\frac{\alpha}{\pi} - 0.32847844400(\frac{\alpha}{\pi})^2 + 1.181234017(\frac{\alpha}{\pi})^3 - 1.7502(384)(\frac{\alpha}{\pi})^4 + 1.70(3) \times 10^{-12} \quad , \tag{1.7}$$

where the hadronic and weak contributions are also accounted for, with the observed value $a_e^{exp} = 0.0011596521883(42)$ to find [3]

$$\alpha^{-1}(a_e) = 137.03599875(52) \quad . \tag{1.8}$$

This value is six times more accurate than the other best assessment via the quantum Hall effect, which returns

$$\alpha^{-1}(qH) = 137.03600300(270) \quad . \tag{1.9}$$

As discussed above, the QED contributions to a_μ are the same as for the electron however, the heavy leptons are also allowed inside the loop this time. The overall QED contribution to a_μ then reads [4]

$$a_\mu^{QED} = 11658471.809(0.016) \times 10^{-10} \quad . \tag{1.10}$$
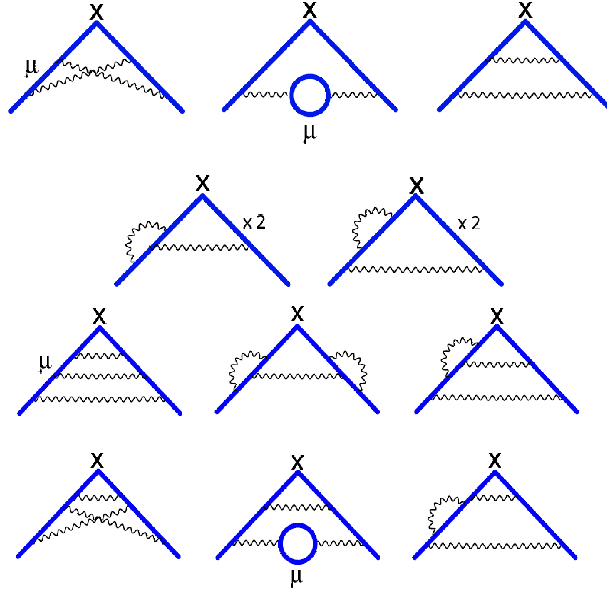
3

Figure 2: Typical second and third order QED loop corrections. Figure from [2].

On the other hand, a_μ is much more sensitive to all three types of effects accounted above, and even to physics beyond the Standard Model due to the higher mass of the muon [1, 2].

The Electroweak contribution to a_μ is divided into two parts, one and two–loop contributions as shown in Figure 3, so that

$$a_\mu^{EW} = a_\mu^{W(1)} + a_\mu^{W(2)} \ , \tag{1.11}$$

which results in

$$
\begin{aligned}
a_\mu^{EW(1)} &= 19.48 \times 10^{-10} \\
a_\mu^{EW(2)} &= -4.07(0.1)(0.18) \times 10^{-10} \\
a_\mu^{EW} &= 15.4(0.1)(0.2) \times 10^{-10} \ .
\end{aligned}
\tag{1.12}
$$

Both the QED and electroweak contributions can be calculated to high precision. In contrast, the hadronic contribution to a_μ cannot be accurately evaluated from low-energy quantum chromodynamics (QCD), and leads to the dominant theoretical uncertainty on the Standard-Model prediction [2]. In fact, since effects of the energies higher than the muon mass are suppressed by powers of (m_μ/M), the relevant QCD contributions to a_μ are in the non perturbative regime. Nevertheless, there exists a consistent theory to control strong interaction dynamics at very low energies, which is called chiral perturbation theory (ChPT) [5] and will be discussed in Sec. 2.4.

The hadronic contribution is divided in two parts: the hadronic vacuum polarization contribution Figure 4, and the HLL, Figure 5, that is
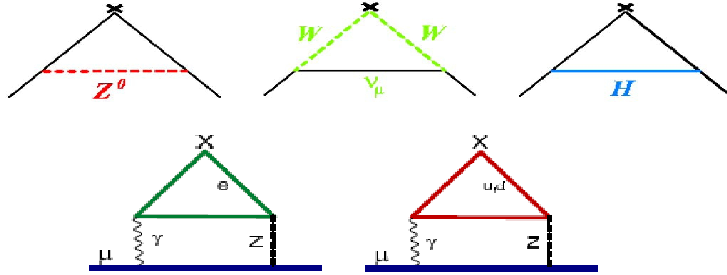
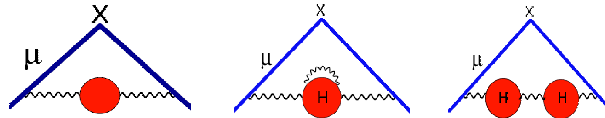Figure 3: Electroweak one loop and two loop contributions to a_μ. Figure from [2].

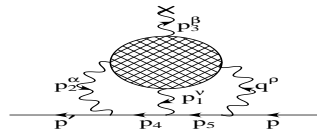Figure 4: The hadronic vacuum polarization contribution, lowest and higher orders. Figure from [2]
.

Figure 5: Hadronic light by light contribution. Figure from [6].

$$a_\mu^{had} = a_\mu^{(hvp)} + a_\mu^{(HLL)} \ . \tag{1.13}$$

The vacuum polarization is divided into the leading order and next-to-leading order, whose contributions are [7]

$$a_\mu^{Had,LO} = 690.9(4.4) \times 10^{-10} \tag{1.14}$$

and

$$a_\mu^{Had,HO} = -9.8(0.1) \times 10^{-10} \ . \tag{1.15}$$

The part we are interested in in this work, is the hadronic light by light scattering, which, contrary to the vacuum polarization part, can not be expressed fully in terms of any experimental data and should be dealt with only theoretically and hence, it can be a source of more serious errors [1] and makes the result model dependent. It consists of three contributions, the quark loop, the pion exchange and the charged pion (Kaon) loop [2]. Due to considerations of the Ref. [8], the estimation of the HLL contribution to the muon $g - 2$ is

$$a_\mu^{(h.L \times L)} = (10.5 \pm 2.6) \times 10^{-10} \ , \tag{1.16}$$

which is suffering from a large error, as discussed above.

Calculating the HLL part is the trickiest. Although, ChPT is a reliable theory of hadrons at low energies, its usage for the pion exchange brings about divergences and one should resort to certain models to get rid of them. One can just introduce some cut off energy, but, the way to do it systematically is to cover the photon legs with vector mesons. These vector mesons cure the infinities similar to what the Pauli Villars method does in QFT, although the Pauli Villars is a pure mathematical manipulation, while vector mesons are observable physical entities. There are certain models to do the job (below). Historically, after Ref. [9] calculated the HLL part via the naive VMD approach, which does not obviously respect the electromagnetic Ward identities [10], the first thorough consideration, compatible with the Ward identities, was by Bijnens, Pallante and Prades [11, 12] via the Extended Nambu–Jona–Lasinio approach, assuming full VMD. The other was by Hayakawa, Kinoshita and Sanda [13] using the HLS model. Then, Knecht–Nyffeler recalculated the $\pi_0, \eta, \eta\prime$ exchange contribution via the quark–hadron duality in the large N_c limit of QCD [14], and found a sign difference with the previous results. Subsequently authors of both previous works found a sign mistake which was corrected [15]. Meanwhile, afterwards, matching between the short and the long distance behavior of the light-by-light scattering amplitude, Melnikov and Vainshtein found some corrections [16].

However, as mentioned above, the HLL contribution consists of three parts among which, we are interested in the charged pion loop correction in this work. The reason is, as can be seen from Table 1, different approaches to this part led to very different results. In fact, when the vector mesons are introduced into the calculation, one expects that results are heavily suppressed, compared to the bare pion loop case. However, as both VMD and HLS models use this mechanism, one might wonder, why the full VMD result is about three times larger than the one from the HLS one. This is the main question which is tried to be answered in this work.
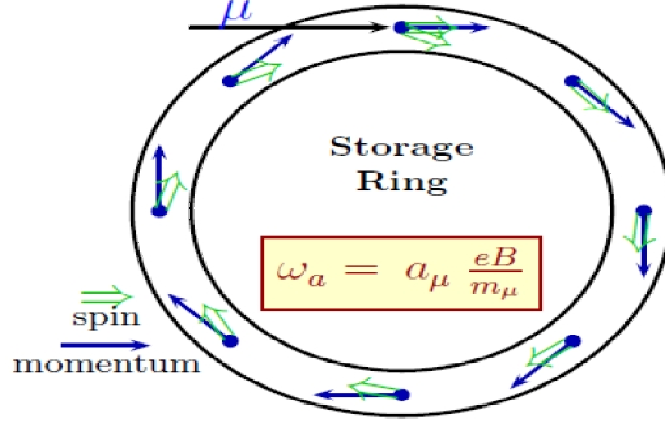
Figure 6: Spin precession in the $g - 2$ ring. Figure from [1].

1.2 Experiment

A diagrammatic scheme of the a_μ measurement is shown in Figure 6 [1]. To measure the magnetic anomaly an electric field $\mathbf{E}$ and/or a magnetic field $\mathbf{B}$ must be applied. The general formula, derived by Michel and Telegdi [3] in 1959 for this purpose, reads

$$\boldsymbol{\omega_a} = \boldsymbol{\omega_s} - \boldsymbol{\omega_c} = -\frac{e}{m_\mu c}\left\{ a_\mu \mathbf{B} - \left[a_\mu + \frac{1}{1-\gamma^2}\right]\boldsymbol{\beta}\times\mathbf{E}\right\} - \frac{2d_\mu}{\hbar}\{\boldsymbol{\beta}\times\mathbf{B}+\mathbf{E}\}\ , \qquad (1.17)$$

where $\omega_c = eB/m_\mu\gamma$ is the cyclotron frequency, $\omega_s = eB/m_\mu\gamma + a_\mu eB/m_\mu$, $\gamma = 1/\sqrt{1-v^2}$ and v the muon speed. If one forgets about the electric dipole moment of the muon, d_μ, so that ω_a is independent of d_μ, and chooses γ such that $a_\mu - 1/(\gamma^2 - 1) = 0$, which corresponds to the energy 3.1 GeV, called the magical energy, the measurement of a_μ reduces to measuring the magnetic field and the value of ω_a. As for ω_a, one should note that the direction of the muon spin is determined by detecting the electrons resulting from the decay $\mu^- \to e^- + \nu_e + \bar{\nu}_\mu$, or positrons from the decay of μ^+ as shown in Figure 7. The number of electrons detected with an energy above some threshold E_t, decreases exponentially with time as shown in Figure 8, according to the formula

Charged pion and Kaon Loop Contributions	$a_\mu \times 10^{10}$
Bijnens, Pallante and Prades(Full VMD)	-1.9 ± 0.5
Hayakawa and Kinoshita (HGS)	-0.45 ± 0.85
Kinoshita, Nizic and Okamoto(Naive VMD)	-1.56 ± 0.23
Kinoshita, Nizic and Okamoto(Scalar QED)	-5.47 ± 4.6

Table 1: Results of different approaches to the charged pion loop HLL contribution to a_μ [6, 9, 13] .
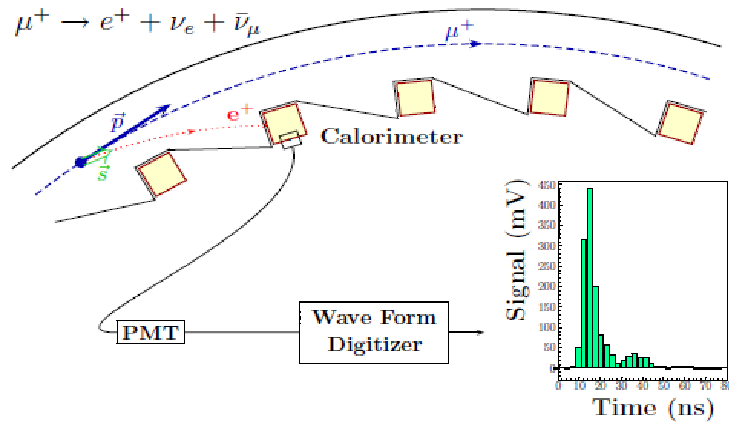
Figure 7: Decay of μ^+ and detection of the emitted e^+. Figure from [1].
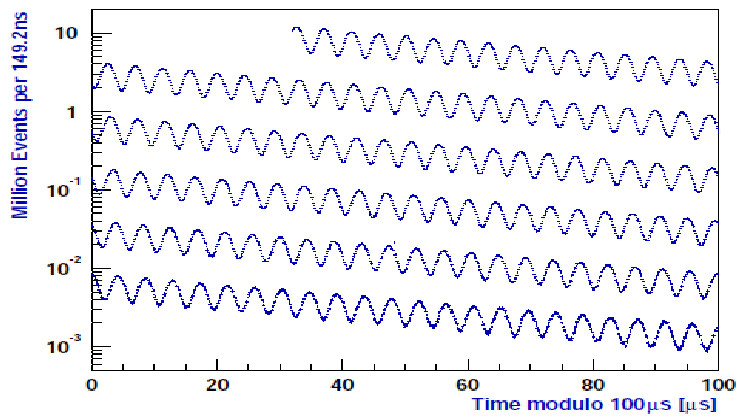

Figure 8: Distribution of counts versus time. Figure from [1].

$$N_e(t) = N_0(E_t)e^{-t/\gamma\tau_\mu} \left\{ 1 + A(E_t)\cos[(\omega_a)t + \Phi(E_t)] \right\} \ , \tag{1.18}$$

where τ_μ is the muon's lifetime in the laboratory frame. This allows one to extract ω_a. Then, one uses the relation

$$B = \frac{\omega_p}{2\mu_p} \ , \tag{1.19}$$

between the Larmor spin precession angular velocity of the proton, ω_p, the proton Bohr magneton, μ_p, and the magnetic field B, to obtain

$$a_\mu = \frac{R}{\lambda - R} \ , \tag{1.20}$$

where $R = \omega_a/\omega_p$ and $\lambda = \mu_\mu/\mu_p$ with μ_μ the muon Bohr magneton. The value of λ is measured separately and is used by the experiment to obtain a_μ via the relation (1.20).

Before the E821 experiment at Brookhaven national laboratory between 2001 and 2004 [1], results of a series of measurements accomplished in the Muon Storage Ring at CERN were in good agreement with theoretical predictions of the Standard Model of particle physics, that is

$$a_\mu^{exp} = 1165924.0(8.5) \times 10^{-9} \qquad a_\mu^{th} = 1165921(8.3) \times 10^{-9} \ . \tag{1.21}$$

The BNL experiment managed to improve the CERN experiment 14 fold. The BNL average value is [17]

$$a_\mu = 11659208.0(3.3)[6.3] \times 10^{-10} \ , \tag{1.22}$$

where the uncertainties are statistical and systematic. The comparison between the experimental and theoretical values has been done in Figure 9. As can be seen, judging by the experimental accuracy achieved in the past decade at BNL, a small discrepancy at the 2 to 3 σ level has persisted with the theoretical predictions. This discrepancy is still debated and many conjectures have been made to link it with physics beyond the standard model.

1.3 Overview of this work

However, as mentioned above, the theoretical predictions in the realm of the SM are still obscured by the hadronic calculations. This work will try to address the charged pion loop, as a part of the HLL scattering contribution to a_μ. The structure of this work is as follows. In Sec. 2, QCD and its chiral symmetry will be discussed to give an introduction to ChPT. Sec. 3 is devoted to the Hidden Local Symmetry (HLS) model, as an extension of the ChPT. Sec. 4 will have a closer look into generalized Feynman vertices for different models and some short distance constraints. In Sec. 5 the main body of calculation of a_μ via different models is discussed and Sec. 6 deals with the role of different momentum regions contribution to a_μ. Finally, in Sec. 7 conclusions and prospects are given.
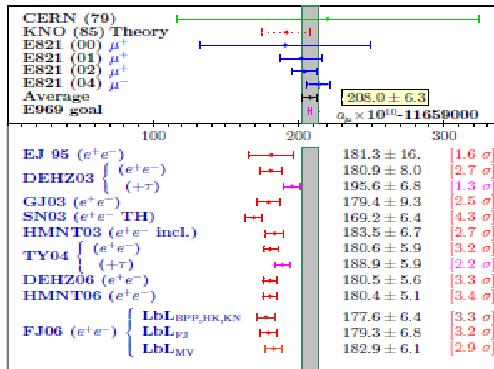
Figure 9: Comparison between the theoretical and experimental values of the a_μ, experimental results in top and theoretical values in below. Table from [18].

2 QCD and chiral Symmetry

2.1 Effective field theory

There is a folklore theorem ascribed to Weinberg which states [19]: For a given set of asymptotic states, perturbation theory with the most general Lagrangian containing all the terms allowed by the assumed symmetries will yield the most general S-matrix elements consistent with analyticity, perturbative unitarity, cluster decomposition and the assumed symmetries. In other words, regardless of the underlying theory, when the degrees of freedom and the symmetries relevant to the energy scale at hand are known, the effective Lagrangian built based on them will address the same physics as the underlying theory. If a small parameter, λ is also realized in the effective theory, one can conduct perturbative calculations upon this parameter. Having this in mind, one would go ahead with constructing an effective theory of strong interactions in low energies where the original QCD Lagrangian runs into problems due to the fact that in the regime $p^2 \ll 1$ GeV squared, where the meson dynamics take place, the QCD coupling constant is large. In this energy regime, the fundamental particles are hadrons rather than quarks and gluons. To build a Lagrangian for a process happening at a scale $p \ll \Lambda$, one can use a expansion in powers of p/Λ where Λ is the cut-off energy of the model. Then, the Lagrangian could be organized as a series of growing powers of momenta, i.e. of derivatives as

$$\mathcal{L} = \mathcal{L}_2 + \mathcal{L}_4 + \cdots + \mathcal{L}_{2n} + \cdots \ , \tag{2.1}$$

where the subscript indicates the number of derivatives. After building the Lagrangian like this, one should use Weinberg power counting to realize to which order a given diagram

Figure 10: Left is the interaction, mediated via the σ particle, right is the same interaction when the mediator has been integrated out.

belongs. Based on the Weinberg power counting scheme, the most important contribution to a given scattering comes from the tree level diagram $\mathcal{L}_2$. The contribution from one loop diagrams is suppressed with respect to tree level and is the same size as the level of contribution from the lagrangian $\mathcal{L}_4$. The formula determining the power counting quantitatively for a given diagram is

$$D = 2 + \sum_{n=1}^{\infty} 2(n-1)N_{2n} + 2N_L \quad , \tag{2.2}$$

where N_{2n} is the number of vertices originating from $\mathcal{L}_{2n}$ and N_L is the number of loops.

2.2 Linear sigma model

To understand how an effective theory can describe dynamics correctly, forgetting about the underlying theory, we digress to the linear sigma model as an example. Let's start with the linear sigma model Lagrangian

$$L = \frac{1}{2}\partial_\mu \boldsymbol{\phi} \cdot \partial^\mu \boldsymbol{\phi}^T - \mu \left(\boldsymbol{\phi} \cdot \boldsymbol{\phi} - a^2 \right)^2 \quad , \tag{2.3}$$

Where the vector field $\boldsymbol{\phi} = (\phi_1, \cdots, \phi_N)$ is a N-component real scalar field. The field has a nonzero vacuum expectation value that is $\phi_0^2 = \phi_1^2 + \cdots + \phi_N = a^2$. We assume that among an infinite number of ground states that satisfy this condition, one of them is chosen dynamically so that, the symmetry is spontaneously broken to the sub group $H \equiv O(N-1)$. This leads to generation of $N-1$ Goldstone bosons according to the Goldstone theorem [20], which are taken to be π^i. Taking a simple choice $\boldsymbol{\phi}_0 = (a, 0, .., 0)$ and expanding $\boldsymbol{\phi}$ around $\boldsymbol{\phi}_0$, assuming $\sigma \ll a$ as the parameter of expansion and then integrating out the σ field, one finds the corresponding effective Lagrangian of the non linear sigma model. In Figure 10 the difference between the case when the sigma particle exists and when it is integrated out in the limit of $p^2/m_\sigma^2 \ll 1$ is depicted.

2.3 Chiral symmetry

Returning to QCD, one can observe that the degrees of freedom to be dealt with at low energy, namely baryons and mesons are quite different from quarks and gluons which are the main players at high energies and the method described for the sigma model to integrate

out the heavy field and build up an effective theory does not seem to be applicable here. However, the fact that there exists an energy gap between the family of pseudo scalar mesons and the rest of the hadrons, and that they can be accounted for as Goldstone bosons of a broken symmetry, encourages us to look for an effective field theory to describe their interactions [5]. The QCD lagrangian is

$$L = \sum_{flavors} \bar{\psi}(i\gamma^\mu \partial_\mu + g_s A^\mu \gamma_\mu - m_i)\psi_i - \frac{1}{4}G_{\mu\nu}G^{\mu\nu} \ , \tag{2.4}$$

where A^μ is the gluon field and $G_{\mu\nu}$ is the gluon field strength tensor with the definition

$$G_{\mu\nu} = \partial_\mu A_\nu - \partial_\nu A_\mu - g_s f A_\mu A_\nu \ , \tag{2.5}$$

with the f coefficients the structure constants of the group $SU(3)_{colour}$. One can define the left handed and right handed fields as

$$\psi_R = \frac{1}{2}(1+\gamma_5)\psi \qquad \psi_L = \frac{1}{2}(1-\gamma_5)\psi \tag{2.6}$$

and $\psi = \psi_L + \psi_R$. The QCD Lagrangian when written in terms of ψ_L and ψ_R is

$$\begin{aligned} L &= \sum_{flavors} \bar{\psi}_L(i\gamma^\mu \partial_\mu + g_s A^\mu \gamma_\mu)\psi_{iL} \\ &+ \bar{\psi}_R(i\gamma^\mu \partial_\mu + g_s A^\mu \gamma_\mu)\psi_{iR} - m_i\bar{\psi}_{iL}\psi_{iR} - m_i\bar{\psi}_{iR}\psi_{iL} - \frac{1}{4}G_{\mu\nu}G^{\mu\nu} \ . \end{aligned} \tag{2.7}$$

If one drops the mass terms the Lagrangian is invariant under following transformations

$$\psi_{iL} \to \exp(-i\alpha_L \cdot \lambda)\psi_{iL} \qquad \psi_{iR} \to \exp(-i\alpha_R \cdot \lambda)\psi_{iR} \ , \tag{2.8}$$

where $\lambda^a(a = 1, 2, \cdots, 8)$ are the $SU(3)$ Gell-Mann matrices in the flavor indices. The Lagrangian is said to have an approximate symmetry $G = SU(3)_L \times SU(3)_R$ or chiral symmetry. Of course quarks are massive and the chiral symmetry is not realized fully in nature however, for three lightest quarks u, d, s, it could be assumed to hold approximately. But as this symmetry is not visible in the spectrum of light hadrons [5], it should be spontaneously broken in nature due to some spontaneous symmetry breaking (SSB) mechanism. This leads to the global symmetry $G = SU(3)_L \times SU(3)_R$ to be reduced to the subgroup $H = SU(3)_V$. This being the case, the Goldstone theorem dictates that the difference between the original number of generators and the final ones, should have turned into Goldstone bosons. In the case at hand the number of Goldstone bosons is 8. As the chiral symmetry is also broken explicitly due to the quark masses in the QCD Lagrangian, the bosons could be recognized as the pseudo scalar mesons, which have acquired a small mass due to this explicit symmetry breaking.

2.4 ChPT

2.4.1 Lowest order

Now that the ground have been laid, one can go ahead by constructing an effective QCD theory at low energies. The most general Lagrangian invariant under Lorentz and chiral transformations in the lowest order has the form [21]

$$\mathcal{L}_2 = \frac{F_0^2}{4}[tr(D_\mu U^\dagger D^\mu U) + 2B_0 tr(UM^\dagger + MU^\dagger)] \ , \tag{2.9}$$

where F_0 is the pion decay constant in the limits of the massless pion, B_0 is related to the chiral quark condensate and U can be shown to be the $SU(3)$ matrix, written in terms of the Goldstone fields as

$$U = \exp{(iF_0\phi)} \ , \tag{2.10}$$

where

$$\phi = \begin{pmatrix} \frac{1}{\sqrt{2}}\pi^0 + \frac{1}{\sqrt{6}}\eta & \pi^+ & K^+ \\ \pi^- & -\frac{1}{\sqrt{2}}\pi^0 + \frac{1}{\sqrt{6}}\eta & K^0 \\ K^- & \bar{K}^0 & -\frac{2}{\sqrt{6}}\eta \end{pmatrix} \tag{2.11}$$

The covariant derivative is

$$D_\mu U = \partial_\mu U - il_\mu U + iU r_\mu \ , \tag{2.12}$$

with right and left external fields reducing to

$$\begin{aligned} l_\mu &= -eQA_\mu \\ r_\mu &= -eQA_\mu \ , \end{aligned} \tag{2.13}$$

for this work with e, the electromagnetic coupling and

$$Q = \frac{1}{3}\begin{pmatrix} 2 & 0 & 0 \\ 0 & -1 & 0 \\ 0 & 0 & -1 \end{pmatrix} \ .$$

Now let's see how can one actually calculate with these tools. To find the amplitude for the scattering $\gamma(q, \varepsilon) \to \pi(p) + \pi(p')$, one has

$$r_\mu = l_\mu = -eQA_\mu \tag{2.14}$$

and hence

$$\begin{aligned} D_\nu U &= \partial_\nu U + ieA_\nu[Q, U] \\ D_\nu U^\dagger &= \partial_\nu U^\dagger + ieA_\nu[Q, U^\dagger] \ . \end{aligned} \tag{2.15}$$

13

Then, starting from the lowest order Lagrangian the corresponding term is

$$
\begin{aligned}
\frac{F^2}{4}\langle D_\mu U (D^\mu U)^\dagger\rangle \;=\;& \frac{F^2}{4}\langle \partial^\mu U \partial^\mu U^\dagger\rangle \\
& - ieA_\mu \frac{F^2}{4}\langle Q[(\partial^\mu U U^\dagger - U^\dagger \partial^\mu U)]\rangle \\
& - A_\mu A^\mu \frac{F^2}{4}\langle [Q,U][Q,U^\dagger]\rangle \; .
\end{aligned}
\tag{2.16}
$$

Putting in from (2.11) and keeping terms only up to second order of ϕ, the second term reads

$$
\mathcal{L} = -e\frac{i}{2}A_\mu\langle Q[\partial^\mu\phi,\phi]\rangle \; .
\tag{2.17}
$$

Inserting from (2.11) only for the pion field of ϕ one gets

$$
Q[\partial^\mu\phi,\phi] = \begin{pmatrix} 2(\partial^\mu\pi^+\pi^- - \pi^+\partial^\mu\pi^-) & 0 & 0 \\ 0 & 2(\partial^\mu\pi^-\pi^+ - \pi^-\partial^\mu\pi^+) & 0 \\ 0 & 0 & 0 \end{pmatrix}
\tag{2.18}
$$

and after performing the trace one easily finds

$$
\mathcal{L} = -eiA_\mu(\partial^\mu\pi^+\pi^- - \pi^+\partial^\mu\pi^-) \; .
\tag{2.19}
$$

Hence, the Feynman rule for the scattering $\gamma(q,\varepsilon) \to \pi^+(p) + \pi^-(p')$, using

$$
A_\mu(x) = \int \frac{d^3p}{(2\pi)^3}\frac{1}{\sqrt{2E_\mathbf{p}}}\sum_{r=0}^{3}\left(a^r_\mathbf{p}\varepsilon^r_\mu(p)\exp(-ip\cdot x) + a^{r\dagger}_\mathbf{p}\varepsilon^{r*}_\mu(p)\exp(ip\cdot x)\right)
\tag{2.20}
$$

and

$$
\phi(x) = \int \frac{d^3p}{(2\pi)^3}\frac{1}{\sqrt{2\omega_\mathbf{p}}}\left(a^\dagger_\mathbf{p}\exp(ip\cdot x) + a_\mathbf{p}\exp(-ip\cdot x)\right) \; ,
\tag{2.21}
$$

as the photon and pion field respectively, reads

$$
\mathcal{M} = ie\varepsilon\cdot(p+p')
\tag{2.22}
$$

and the vertex is proportional to

$$
ie(p_\mu + p'_\mu) \; .
\tag{2.23}
$$

Following the same lines for the scattering $\gamma(q,\varepsilon) + \gamma(q',\varepsilon') \to \pi^+(p) + \pi^-(p')$, the Lagrangian becomes

$$
\mathcal{L} = e^2 A_\mu A^\mu \pi^+\pi^-
\tag{2.24}
$$

and the amplitude is

$$
\mathcal{M} = 2ie^2\varepsilon'^{\star}\cdot\varepsilon \; ,
\tag{2.25}
$$

which leads to the vertex

$$
2ie^2 g_{\mu\nu} \; .
\tag{2.26}
$$

14

2.4.2 L_9 and L_{10}

The Lagrangian in order p^4 of ChPT has the form [21]

$$
\begin{aligned}
\mathcal{L}_4 \;=\;& L_1 \langle D_\mu U^\dagger D^\mu U \rangle^2 + L_2 \langle D_\mu U^\dagger D_\nu U \rangle \langle D^\mu U^\dagger D^\nu U \rangle \\
& + L_3 \langle D^\mu U^\dagger D_\mu U D^\nu U^\dagger D_\nu U \rangle + L_4 \langle D^\mu U^\dagger D_\mu U \rangle \langle \chi^\dagger U + \chi U^\dagger \rangle \\
& + L_5 \langle D^\mu U^\dagger D_\mu U (\chi^\dagger U + U^\dagger \chi) \rangle + L_6 \langle \chi^\dagger U + \chi U^\dagger \rangle^2 \\
& + L_7 \langle \chi^\dagger U - \chi U^\dagger \rangle^2 + L_8 \langle \chi^\dagger U \chi^\dagger U + \chi U^\dagger \chi U^\dagger \rangle \\
& - i L_9 \langle F_{\mu\nu}^R D^\mu U D^\nu U^\dagger + F_{\mu\nu}^L D^\mu U^\dagger D^\nu U \rangle \\
& + L_{10} \langle U^\dagger F_{\mu\nu}^R U F^{L\mu\nu} \rangle \,,
\end{aligned}
\tag{2.27}
$$

where the field strength tensor reads

$$
F_{\mu\nu}^{L(R)} = \partial_\mu l(r)_\nu - \partial_\nu l(r)_\mu - i \left[l(r)_\mu, l(r)_\nu \right] \,,
\tag{2.28}
$$

with

$$
\chi = 2 B_0 \left(s + ip \right) \,,
\tag{2.29}
$$

in which s, p, l_μ and r_μ denote the scalar, pseudo scalar, left and right handed external fields, respectively [21]. The terms of interest in this Lagrangian for our purpose are those containing L_9 and L_{10}. These term correspond to the pion charge radius and pion polarizability.

One can rewrite the term containing L_9 as

$$
\begin{aligned}
\mathcal{L}_9 \;=\;& -i \langle F_{\mu\nu R} D_\mu U D_\nu U^\dagger + F_{\mu\nu L} D_\mu U^\dagger D_\nu U \rangle \\
=\;& i \langle D_\mu F_{\mu\nu R} U D_\nu U^\dagger + D_\mu F_{\mu\nu L} U^\dagger D_\nu U \rangle \\
& + i \langle F_{\mu\nu R} U D_\mu D_\nu U^\dagger + F_{\mu\nu L} U^\dagger D_\mu D_\nu U \rangle = \mathcal{L}_9^1 + \mathcal{L}_9^2 \,.
\end{aligned}
\tag{2.30}
$$

The second term can be written as

$$
\mathcal{L}_9^2 = \frac{i}{2} \langle F_{\mu\nu R} U [D_\mu, D_\nu] U^\dagger + F_{\mu\nu L} U^\dagger [D_\mu, D_\nu] U \rangle \,,
\tag{2.31}
$$

which using the equalities

$$
[D_\mu, D_\nu] U^\dagger = -i (F_{\mu\nu L} U^\dagger - U^\dagger F_{\mu\nu R}) \qquad [D_\mu, D_\nu] U = -i (F_{\mu\nu R} U - U F_{\mu\nu L}) \,,
\tag{2.32}
$$

takes the same form as $\mathcal{L}_{10}$ in the above Lagrangian. Since we are dealing only with electromagnetic interaction, $F_{\mu\nu L} = F_{\mu\nu R}$ and $\mathcal{L}_9^1$ becomes

$$
\mathcal{L}_9^1 = \langle D_\mu F^{\mu\nu} [U D_\nu U^\dagger + U^\dagger D_\nu U] \rangle \,,
\tag{2.33}
$$

Which upon use of the relation (2.15) reads

$$
\begin{aligned}
\mathcal{L}_9^1 = \langle D_\mu F_{\mu\nu} \Big[U \partial U^\dagger \;+\;& ie A_\nu U [Q, U^\dagger] \\
U^\dagger \partial \nu U \;+\;& ie A_\nu U^\dagger [Q, U] \Big] \rangle \,.
\end{aligned}
\tag{2.34}
$$

15

Then using the definition (2.10), expanding U and keeping terms up to the order ϕ^2 one finds

$$
\begin{aligned}
U\partial_\nu U^\dagger &= -\partial_\nu U U^\dagger = -i\frac{\partial_\nu\phi}{F_0} \\
U^\dagger\partial_\nu U &= -\partial_\nu U^\dagger U = i\frac{\partial_\nu\phi}{F_0}
\end{aligned}
\tag{2.35}
$$

and

$$
\begin{aligned}
U[Q, U^\dagger] &\simeq [Q, \frac{(i\phi)^2}{2}] + i\phi[Q, -i\phi] \\
U^\dagger[Q, U] &\simeq [Q, \frac{(i\phi)^2}{2}] - i\phi[Q, i\phi] \ .
\end{aligned}
\tag{2.36}
$$

Using relations (2.11) and (2.12), the final result is

$$
\mathcal{L}_9^1 = -e\partial_\mu f^{\mu\nu}\Big[2(\pi^+\partial_\nu\pi^- - \pi^-\partial_\nu\pi^+) - 2ieA_\nu\pi^+\pi^-\Big] \ .
\tag{2.37}
$$

The second part of the Eq. (2.30) can also be calculated in the same way to give

$$
\mathcal{L}_9^2 = -4e^2 f_{\mu\nu}f^{\mu\nu}\pi^+\pi^- \ ,
\tag{2.38}
$$

where $F_{\mu\nu} = -eQf_{\mu\nu}$ is assumed and

$$
\begin{aligned}
f_{\mu\nu}f^{\mu\nu} &= (\partial_\mu A_\nu - \partial_\nu A_\mu)(\partial^\mu A^\nu - \partial^\nu A^\mu) \\
&= \partial_\mu A_\nu\partial^\mu A^\nu - \partial_\nu A_\mu\partial^\nu A^\mu - \partial_\nu A_\mu\partial^\mu A^\nu + \partial_\nu A_\mu\partial^\nu A^\mu \ .
\end{aligned}
\tag{2.39}
$$

One can also derive the term corresponding to $\mathcal{L}_{10}$ similarly. The only remaining task is to derive the part related to $F_{\mu\nu}$ and extract the Feynman rules. For example for the $\gamma\gamma\pi\pi$ process

$$
\mathcal{M} = \langle kk'|\partial_\mu A_\nu\partial^\mu A^\nu\pi^+\pi^-|pp'\rangle \ ,
\tag{2.40}
$$

which via using relation (2.20) and (2.21), leads to the following invariant amplitude

$$
\mathcal{M} = 4\varepsilon_\mu(p)\varepsilon^\mu(p')p_\mu p'^\mu - 4p_\mu p'^\nu\varepsilon_\nu(p)\varepsilon^\mu(p') \ .
\tag{2.41}
$$

To get a better understanding of what L_9 and L_{10} actually represent, the charge radius of the pion is related to its electromagnetic form factor in the low energy region via the definition [22]

$$
F^{\pi^\pm}(p^2) = 1 + \frac{p^2}{6}\langle r^{\pi^2}\rangle + \cdots \ .
\tag{2.42}
$$

Comparing this with the pion form factor in the low energy limit one gets

$$
\langle r^{\pi^2}\rangle = \frac{3a}{m_\rho^2} \ .
\tag{2.43}
$$

Meanwhile, it could be shown that [23], $L_9 \propto 1/m_\rho^2$ and hence, L_9 is proportional to the pion charge radius. Using similar arguments, L_{10} can be shown to be related to the pion polarizability.

16

3 Hidden local symmetry model

As the Hidden Local Symmetry (HLS) is used extensively in this work, we give a brief introduction to it in this section. In fact, the HLS considers vector mesons as its gauge bosons, achieving mass via eating up the Goldstone bosons appearing as a result of breaking of the hidden symmetry, which is added to the chiral symmetry of the ChPT Lagrangian [24]. Hence this model is a kind of generalization of perturbation theory. Indeed, ChPT at its tree level only covers the threshold energy and even after adding the loop corrcetions, the energy it covers is fully below the chiral symmetry breaking energy around 1GeV [22]. As the energy grows the ρ meson should be inevitably considered. That is where the HLS takes center stage. There are also some other compatible models discussed in the literature [22].

As discussed above, symmetry of ChPT is of the type $G_{global} = SU(N_f)_L \times SU(N_f)_R$, which in the HLS model is extended to $G_{global} \times H_{local}$ with $H = SU(N_f)_V$. It is interesting to mention that the HLS model reduces to ChPT in the low energy region when the vector meson is integrated out. In the HLS model the variable U of ChPT, introduced in the relation (2.10) is divided into two parts

$$U = \xi_l^\dagger \xi_r \ . \tag{3.1}$$

These new variables can be parameterized as

$$\xi_{l,r} = \exp\left(i\sigma/F_\sigma\right)\exp\left(\pm i\pi/F_\pi\right) \qquad \text{with} \qquad \left[\pi = \pi^a T_a, \sigma = \sigma^a T_a\right] \ , \tag{3.2}$$

where π denotes the Goldstone bosons of the global symmetry and have the same definition as before, while σ denotes those of the local symmetry. These are the Goldstone bosons absorbed by the vector mesons to get massive. Also, F_π and F_σ are the corresponding decay constants respectively and T_a are the generators of the group. Then, one can introduce the covariant derivative including the external fields

$$D_\mu \xi_l = \partial \xi_l - iv_\mu \xi_l + i\xi_l l_\mu \qquad D_\mu \xi_r = \partial \xi_r - iv_\mu \xi_r + i\xi_r r_\mu \ , \tag{3.3}$$

where r and l are the same as in (2.13), with the gauge fields of the H_{local} defined as[1]

$$\rho_\mu = \frac{v_\mu^a}{g} T_a = \frac{1}{\sqrt{2}} \begin{pmatrix} \frac{1}{\sqrt{2}}\left(\rho_\mu^0 + \omega_\mu\right) & \rho_\mu^+ & K_\mu^{\star,+} \\ \rho_\mu^- & -\frac{1}{\sqrt{2}}\left(\rho_\mu^0 + \omega_\mu\right) & K_\mu^{\star,0} \\ K_\mu^{\star,-} & \bar{K}_\mu^{\star,0} & \phi_\mu \end{pmatrix} \ ,$$

satisfying the field strength

$$v_{\mu\nu} = \partial_\mu v_\nu - \partial_\nu v_\mu - i[v_\mu, v_\nu] \ . \tag{3.4}$$

Then, one can build two independent 1-forms out of the above variables

$$\alpha_\perp^\mu(x) = \frac{(D_\mu \xi_r \cdot \xi_r^\dagger - D_\mu \xi_l \cdot \xi_l^\dagger)}{2i} \qquad \alpha_\parallel^\mu(x) = \frac{(D_\mu \xi_r \cdot \xi_r^\dagger + D_\mu \xi_l \cdot \xi_l^\dagger)}{2i} \ . \tag{3.5}$$

---

[1]This does include an extra $U(1)$ global but the ω plays no role in this work.

Using these 1-forms, one can build the lowest order lagrangian including $\xi_{l,r}$ and $D_\mu \xi_{l,r}$ to the lowest derivative as

$$\mathcal{L} = \mathcal{L}_A + a\mathcal{L}_V = F_\pi^2 tr[(\hat{\alpha}_\perp^\mu(x))^2] + F_\sigma^2 tr[(\hat{\alpha}_\parallel^\mu(x))^2] \ , \tag{3.6}$$

where

$$a \equiv F_\sigma^2/F_\pi^2 \ , \tag{3.7}$$

is a constant.

Finally, adding the kinetic term of the gauge bosons, the Lagrangian, in the unitary gauge $\sigma = 0$, takes the form

$$
\begin{aligned}
\mathcal{L} &= \mathcal{L}_A + a\mathcal{L}_V + \mathcal{L}_{int}(V_\mu) \\
&= F_\pi^2 tr[(\hat{\alpha}_\perp^\mu(x))^2] + F_\sigma^2 tr[(\hat{\alpha}_\parallel^\mu(x))^2] - \frac{1}{2g^2} tr[V_{\mu\nu} V^{\mu\nu}] \\
&= tr[\partial_\mu \pi \partial^\mu \pi] + ag^2 F_\pi^2 tr[\rho_\mu \rho^\mu] + 2i\left(\frac{1}{2}ag\right) tr\left[\rho^\mu[\partial_\mu, \pi]\right] \\
&- 2eagF_\pi^2 A^\mu tr[\rho_\mu Q] + 2ie\left(1 - \frac{a}{2}\right) A^\mu tr\left[Q[\partial_\mu, \pi]\right] \\
&+ ae^2 F_\pi^2 A_\mu A^\mu tr[QQ] + \frac{4 - 3a}{12F_\pi^2} tr\left[[\partial_\mu, \pi][\partial_\mu, \pi]\right] + \cdots \ ,
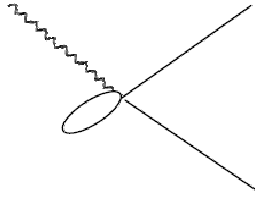\end{aligned} \tag{3.8}
$$

where g is the HLS gauge coupling constant. from this one can easily observe that the vector meson has acquired mass equal to $ag^2 F_\pi^2$ via the Higgs mechanism. Also other couplings could be expressed as

$$
\begin{aligned}
g_{\rho\pi\pi} &= \frac{1}{2}ag \\
g_\rho &= agF_\pi^2 \\
g_{\gamma\pi\pi} &= \left(1 - \frac{a}{2}\right)e \ .
\end{aligned} \tag{3.9}
$$

The relevant terms of the above Lagrangian for our purpose in this work, are [10]

$$
\begin{aligned}
\mathcal{L}_{int} &= -eg_\rho A^\mu \rho_\mu^0 - ig_{\rho\pi\pi}\rho_\mu^0 \pi^+ \overleftrightarrow{\partial}^\mu \pi^- - ig_{\gamma\pi\pi} A_\mu \pi^+ \overleftrightarrow{\partial}^\mu \pi^- \\
&+ (1 - a)e^2 A^\mu A_\mu \pi^+ \pi^- + 2eg_{\rho\pi\pi} A^\mu \rho_\mu^0 \pi^+ \pi^- \ .
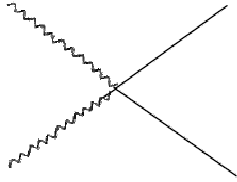\end{aligned} \tag{3.10}
$$

It should be mentioned that the crucial property of this Lagrangian, regarding our consideration of the HLL scattering is that it does not have a $\rho^0\rho^0\pi^+\pi^-$ term. Corresponding diagrams to each of the above terms are depicted in Figure 11. Another property of the HLS lagrangian is that for the $a = 2$ case it reduces to the VMD for the pion single photon coupling, still it is different from the full VMD version which includes the $\rho\rho\pi\pi$ vertex as well.
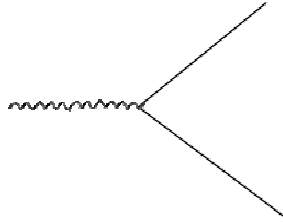
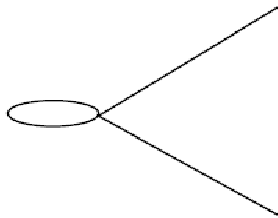(a) $2eg_{\rho\pi\pi}A^\mu\rho_\mu^0\pi^+\pi^-$

(b) $-eg_\rho A^\mu\rho_\mu^0$

(c) $(1-a)e^2A^\mu A_\mu\pi^+\pi^-$

(d) $-ig_{\gamma\pi\pi}A_\mu(\pi^+\partial^\mu\pi^- - \pi^-\partial^\mu\pi^+)$

(e) $-ig_{\rho\pi\pi}\rho_\mu(\pi^+\partial^\mu\pi^- - \pi^-\partial^\mu\pi^+)$

Figure 11: Different HLS Lagrangian terms with the corresponding Feynman diagrams.

19

4 $\gamma\pi^+\pi^-$ and $\gamma\gamma\pi^+\pi^-$ vertices

Up to this point necessary ingredients of a more through discussion of the HLL contribution to a_μ are introduced. As discussed in the introduction, to cure the infinities one has to introduce vector mesons in the calculation of the pion exchange, and this could be done via VMD models or the HLS model. At this point one is ready to consider what kind of change happens to the point diagrams of the ChPT Lagrangian mentioned in the Sec. 2.4, when the HLS or VMD models are taken into account. In the naive VMD model, one just replaces the photon propagator with the term below

$$\frac{ig_{\mu\nu}}{q^2} \to \frac{ig_{\mu\nu}}{q^2} + \frac{-ig_{\mu\nu}}{q^2 - m_\rho^2} \equiv \frac{ig_{\mu\nu}}{q^2}\frac{m_\rho^2}{q^2 - m_\rho^2} \quad . \tag{4.1}$$

However, this simple model is not compatible with Ward identities [10].

To proceed more systematically, one can note that the amplitude corresponding to the γ to ρ to $\pi\pi$, depicted in the right of the Figure 12 is

$$\mathcal{M} = ie\varepsilon \cdot (p + p')\frac{a}{2}\frac{(-i)(-i)(m_\rho^2 g_{\mu\nu} - q_\mu q_\nu)}{(q^2 - m_\rho^2)} \tag{4.2}$$

and hence, one only needs to multiply the vertex of $\gamma\pi\pi$ from (2.23) with

$$(1 - \frac{a}{2})g_{\mu\bar{\mu}} - \frac{a}{2}\frac{m_\rho^2 g_{\mu\bar{\mu}} - q_\mu q_{\bar{\mu}}}{q^2 - m_\rho^2} = g_{\mu\bar{\mu}} - \frac{a}{2}\frac{q^2 g_{\mu\bar{\mu}} - q_\mu q_{\bar{\mu}}}{q^2 - m_\rho^2} \quad , \tag{4.3}$$

to find the equivalent vertex including both diagrams shown in Figure 12. Following the same lines, the amplitude corresponding to Figure 13, is found by multiplying the $\gamma\gamma\pi\pi$ vertex (2.26) with

$$(1 - a)g_{\mu\bar{\mu}}g_{\nu\bar{\nu}} - \frac{a}{2}g_{\nu\bar{\nu}}\left(\frac{m_\rho^2 g_{\mu\bar{\mu}} - q_\mu q_{\bar{\mu}}}{q^2 - m_\rho^2}\right) - \frac{a}{2}g_{\mu\bar{\mu}}\left(\frac{m_\rho^2 g_{\nu\bar{\nu}} - q_\nu q_{\bar{\nu}}}{q^2 - m_\rho^2}\right)$$

$$= \left[g_{\mu\bar{\mu}}g_{\nu\bar{\nu}} + g_{\mu\bar{\mu}}\frac{a}{2}\frac{p^2 g_{\nu\bar{\nu}} - p_{\bar{\nu}}p_\nu}{m_\rho^2 - p^2} + g_{\nu\bar{\nu}}\frac{a}{2}\frac{q^2 g_{\mu\bar{\mu}} - q_{\bar{\mu}}q_\mu}{m_\rho^2 - q^2}\right] \quad . \tag{4.4}$$
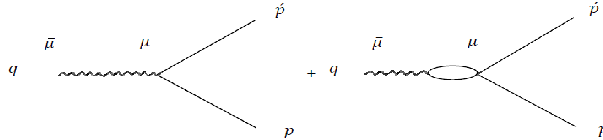

Figure 12: The equivalent vertex of the $\gamma\pi\pi$ in the HLS model.
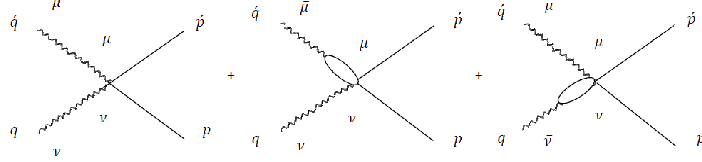
Figure 13: The equivalent vertex of $\gamma\gamma\pi\pi$ in the HLS.

In the full VMD version, one multiplies the point like $\gamma\pi\pi$ vertex with

$$\frac{m_\rho^2 g_{\mu\nu} - m_\rho^2 q_\mu q_\nu}{m_\rho^2 - q^2} \tag{4.5}$$

and the $\gamma\gamma\pi\pi$ vertex of (2.26) with the term

$$\frac{m_\rho^2 g_{\nu\bar\nu} - p_{\bar\nu}p_\nu}{m_\rho^2 - p^2} \frac{m_\rho^2 g_{\mu\bar\mu} - q_{\bar\mu}q_\mu}{m_\rho^2 - q^2} \quad . \tag{4.6}$$

These new vertices are fully gauged and chiral invariant as mentioned in Ref. [12]. One can also follow the same procedure to retrieve the desired Feynmen rules for the L_9 and L_{10}. The extension of the point vertex $\gamma\pi\pi$ is achieved when multiplied with

$$g_{\mu\bar\mu} + L_9 \left(q^2 g_{\mu\bar\mu} - q_\mu q_{\bar\mu} \right) \tag{4.7}$$

and the amplitude corresponding to the $\gamma\gamma\pi\pi$ vertex, including the p^4 corrections, should be multiplied with

$$\begin{aligned} g_{\mu\bar\mu} g_{\nu\bar\nu} \quad & + \quad g_{\mu\bar\mu} L_9 \left(p^2 g_{\nu\bar\nu} - p_{\bar\nu}p_\nu \right) + g_{\nu\bar\nu} L_9 \left(q^2 g_{\mu\bar\mu} - q_{\bar\mu}q_\mu \right) \\ & + \quad (L_9 + L_{10}) \left(q \cdot p g_{\mu\bar\mu} g_{\nu\bar\nu} - g_{\mu\nu} p_{\bar\mu} q_{\bar\nu} \right) \ , \end{aligned} \tag{4.8}$$

where L_9 and L_{10} are constants involved in the Lagrangian (2.27).

4.1 High energy limit

In this section, the high energy limits and the matching with low energy limits are considered.
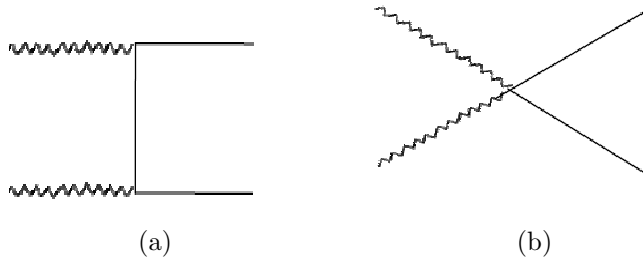
Figure 14: The $\gamma\gamma\pi\pi$ vertex.

It can be shown that the $\gamma\gamma\pi\pi$ amplitude for two high energy photons with momenta $P_1 \simeq -P_2 \simeq P$ is proportional to $1/P^2$. This is done by using the operator product expansion for two vector currents and showing that the matrix element of the leading part which is proportional to an axial current vanishes. Hence, when $P \to \infty$ the amplitude vanishes. The amplitude corresponding to the diagram 14 is

$$\mathcal{M} = ie^2 \left\{ \frac{(P_{1\mu} - 2K_{1\mu})(P_{2\nu} - 2K_{2\nu})}{(P_2 - K_2)^2 - m_\pi^2} + \frac{(P_{2\nu} - 2K_{1\nu})(P_{1\mu} - 2K_{2\mu})}{(P_1 - K_2)^2 - m_\pi^2} - 2g_{\mu\nu} \right\} \ . \tag{4.9}$$

For $P_1 \simeq -P_2 \simeq P \to \infty$ this reads

$$\mathcal{M} = \left(2g_{\mu\nu} - 2\frac{P_\mu P_\nu}{P^2} \right) \ , \tag{4.10}$$

which does not vanish fast enough. For the VMD case the above amplitude should be multiplied with (4.6). The resulting amplitude vanishes at order P^0. Now let us examine the HLS case. Then, the first and second term of (4.9) are multiplied with (4.3) and the third is multiplied with (4.4). In the high energy limit the leading term is

$$\mathcal{M} = 2 \left(g_{\mu\nu} - \frac{P_\mu P_\nu}{P^2} \right)(1 - a) \ . \tag{4.11}$$

This is only satisfied for $a = 1$. However, the case HLS with $a = 2$ does not uphold this condition. Hence, one can infer that something must be wrong with it.

5 Muon magnetic anomaly from light by light amplitude

5.1 General

The response of a muon carrying momentum p to an external electromagnetic field A_μ with momentum transferred $p_3 \equiv p - p'$ is described by the matrix element

$$\mathcal{M} \equiv - \mid e \mid A_\rho \bar{u}(p')\Gamma^\rho(\acute{p}, p)u(p) \ , \tag{5.1}$$

with

$$\Gamma^\rho(p',p) = F_1(p_3^2)\gamma^\rho - \frac{i}{2m_l}F_2(p_3^2)\sigma^{\rho\nu}p_{3\nu} - F_3(p_3^2)\gamma_5\sigma^{\rho\nu}p_{3\nu} + F_4(p_3^2)[p_3^2\gamma^\rho - 2m_l p_3^\rho]\gamma_5 \ . \quad (5.2)$$

The two first form factors are known as the Dirac and the Pauli form factor, respectively. In fact [12], the magnetic moment of the fermion in magnetons is $\mu \equiv 2(F_1(0) + F_2(0))$ and in analogy with the classical limit, described in the introduction, one can define the gyromagnetic ratio as $g \equiv 2\mu$ and the anomalous magnetic moment as $a \equiv (g - 2)/2 = F_2(0)$ [12]. The form factor $F_3(p_3^2)$ can be different from zero provided parity and time reversal invariance are broken and for $F_4(p_3^2)$ to be nonzero, parity invariance should be broken. Therefore, both are absent in our survey. Since the task of computation of $\Gamma_\rho(p',p)$ is very involved especially for higher order corrections, one can project out the form factor of interest, $F_2(p_3^2)$ in our case, and then the general form of the contribution can be shown to be [3]

$$a_\mu^{\text{light}-\text{by}-\text{light}} = -\frac{1}{48m}\text{tr}[(\not p + m)\Gamma^{\lambda\beta}(0)\,(\not p + m)[\gamma_\lambda, \gamma_\beta]] \ . \quad (5.3)$$

Defining the four point function $\Pi_{\rho\nu\alpha\lambda}$ as

$$\begin{aligned}
\Pi^{\rho\nu\alpha\lambda}(p_1, p_2, p_3) &= i^3 \int d^4x_1 \int d^4x_2 \int d^4x_3 \exp i\,(p_1 \cdot x_1 + p_2 \cdot x_2 + p_3 \cdot x_3) \\
&\times \ \langle 0 \mid T j_\rho(0) j_\nu(x_1) j_\alpha(x_2) j_\lambda(x_3) \mid 0 \rangle
\end{aligned} \quad (5.4)$$

and using the Ward identity to rewrite it in the form

$$\Pi^{\rho\nu\alpha\lambda}(p_1, p_2, p_3) = -p_{3\beta}\frac{\delta\Pi^{\rho\nu\alpha\beta}(p_1, p_2, p_3)}{\delta p_{3\lambda}} \ , \quad (5.5)$$

the $\Gamma^{\lambda\beta}(0)$ for the Figure 5 writes

$$\begin{aligned}
\Gamma^{\lambda\beta}(p_3) &= |e|^6 \int \frac{d^4p_1}{(2\pi)^4} \int \frac{d^4p_2}{(2\pi)^4}\frac{1}{q^2\,p_1^2\,p_2^2(p_4^2 - m^2)\,(p_5^2 - m^2)} \\
&\times \ \left[\frac{\delta\Pi^{\rho\nu\alpha\beta}(p_1, p_2, p_3)}{\delta p_{3\lambda}}\right]\gamma_\alpha(\not p_4 + m)\gamma_\nu(\not p_5 + m)\gamma_\rho \ .
\end{aligned} \quad (5.6)$$

with $p_4 = p' - p_2$, $p_5 = p - q$. The most formidable task ahead is then to build the relevant four point functions and to calculate the integral (5.6). One should note that this four-point function can be decomposed by using Lorentz covariance as follows

$$\begin{aligned}
\Pi^{\rho\nu\alpha\beta}(p_1, p_2, p_3) &\equiv \Pi^1(p_1, p_2, p_3)g^{\rho\nu}g^{\alpha\beta} + \Pi^2(p_1, p_2, p_3)g^{\rho\alpha}g^{\nu\beta} \\
&+ \ \Pi^3(p_1, p_2, p_3)g^{\rho\beta}g^{\nu\alpha} \\
&+ \ \Pi^{1jk}(p_1, p_2, p_3)g^{\rho\nu}p_j^\alpha p_k^\beta + \Pi^{2jk}(p_1, p_2, p_3)g^{\rho\alpha}p_j^\nu p_k^\beta \\
&+ \ \Pi^{3jk}(p_1, p_2, p_3)g^{\rho\beta}p_j^\nu p_k^\alpha + \Pi^{4jk}(p_1, p_2, p_3)g^{\nu\alpha}p_j^\rho p_k^\beta \\
&+ \ \Pi^{5jk}(p_1, p_2, p_3)g^{\nu\beta}p_j^\rho p_k^\alpha + \Pi^{6jk}(p_1, p_2, p_3)g^{\alpha\beta}p_j^\rho p_k^\nu \\
&+ \ \Pi^{ijkm}(p_1, p_2, p_3)p_i^\rho p_j^\nu p_k^\beta p_m^\alpha \ ,
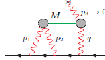\end{aligned} \quad (5.7)$$

Figure 15: The pion exchange HLL contribution to a_μ. Figure from [6].

where $i, j, k, m = 1$, 2 or 3 and repeated indices are summed. There are in total 138 Π-functions. However, due to Ward identities

$$p_{1\nu}\Pi^{\rho\nu\alpha\beta}(p_1, p_2, p_3) = p_{2\alpha}\Pi^{\rho\nu\alpha\beta}(p_1, p_2, p_3) =$$
$$p_{3\beta}\Pi^{\rho\nu\alpha\beta}(p_1, p_2, p_3) = q_\rho\Pi^{\rho\nu\alpha\beta}(p_1, p_2, p_3) = 0 \ , \tag{5.8}$$

all of these functions are not independent and using these identities frequently, the overall number could be reduced to 43 independent $\Pi^{ijkm}(p_1, p_2, p_3)$ functions, 32 of which contribute to a_μ, Ref. [12]. When the functions are found, one should add them up, derivate them with respect to p_3, then set $p_3 = 0$ and put them into the integral (5.6).

5.2 Integration

In this work the main focus is to calculate the contribution of the charged pion loop light by light scattering to a_μ. However, to get familiar with the overall idea behind the mathematical approach, it would be illuminating to start with the simpler calculation for the pion exchange, shown in Figure 15.

5.2.1 Pion exchange

The key object that is used for this case is the $\pi\gamma^\star\gamma^\star$ amplitude, which can be calculated via [1]

$$\int d^4 \ x \exp i \, (p \cdot x) \times \langle 0 \mid T\{j_\mu(x_1)j_\nu(x_2)\} \mid \pi^0(p)\rangle$$
$$= \ \varepsilon_{\mu\nu\alpha\beta}p_1^\alpha p_2^\beta \mathcal{F}_{\pi^0\gamma\gamma}(m_\pi^2, p_1^2, p_2^2) \ , \tag{5.9}$$

where, $\mathcal{F}_{\pi^0\gamma\gamma}$ is the form factor function and p_1 and p_2 are the photon momenta involved in the $\pi^0\gamma\gamma$ vertex. Calculating this amplitude for each of the vertices of the Figure 15, constructing the whole amplitude, taking derivative respect to p_3, putting $p_3 = 0$ and plugging into the relation (5.3) for three different permutations of Figure 15, one finds

$$a_\mu^{LbL} = -e^6 \int \frac{d^4p_1}{(2\pi)^4} \int \frac{d^4p_2}{(2\pi)^4} \frac{1}{p_1^2 p_2^2 (p_1 + p_2)^2 [(p + p_1) - m_\mu^2][(p - p_2) - m_\mu^2]}$$

$$\times \left[\frac{\mathcal{F}_{\pi^{0\star}\gamma^\star\gamma^\star}(p_2^2, p_1^2, q^2)\mathcal{F}_{\pi^{0\star}\gamma^\star\gamma}(p_2^2, p_2^2, 0)}{p_2^2 - m_\pi^2} T_2(p_1, p_2; q) \right.$$

$$+ \left. \frac{\mathcal{F}_{\pi^{0\star}\gamma^\star\gamma^\star}(q^2, p_1^2, p_2^2)\mathcal{F}_{\pi^{0\star}\gamma^\star\gamma}(q^2, q^2, 0)}{q^2 - m_\pi^2} T_1(p_1, p_2; q) \right] \quad , \tag{5.10}$$

with

$$\begin{aligned}
T_1(p_1, p_2; q) = {} & \frac{16}{3}(p \cdot p_1)(p \cdot p_2)(p_1 \cdot p_2) - \frac{16}{3}(p \cdot p_2)^2 p_1^2 \\
& - \frac{8}{3}(p \cdot p_1)(p_1 \cdot p_2)p_2^2 + 8(p \cdot p_2)p_1^2 p_2^2 \\
& - \frac{16}{3}(p \cdot p_2)(p_1 \cdot p_2)^2 + \frac{16}{3}m_\mu^2 p_1^2 p_2^2 \\
& - \frac{16}{3}m_\mu^2 (p_1 \cdot p_2)^2
\end{aligned} \tag{5.11}$$

$$\begin{aligned}
T_2(p_1, p_2; q) = {} & \frac{16}{3}(p \cdot p_1)(p \cdot p_2)(p_1 \cdot p_2) - \frac{16}{3}(p \cdot p_1)^2 p_2^2 \\
& + \frac{8}{3}(p \cdot p_1)(p_1 \cdot p_2)p_2^2 + \frac{8}{3}(p \cdot p_1)(p_1 \cdot p_2)p_2^2 \\
& + \frac{8}{3}(p \cdot p_1)(p_1^2 p_2^2) + \frac{8}{3}m_\mu^2 p_1^2 p_2^2 \\
& - \frac{8}{3}m_\mu^2 (p_1 \cdot p_2)^2 \quad ,
\end{aligned} \tag{5.12}$$

where $q = -(p_1 + p_2)$ has been used in the limit that p_3 vanishes. Also, p is the muon momentum. This is an eight dimensional integral to be done. In general three of the integrations can be done analytically and one is left with a five dimensional integral consisting of three angles and two moduli. Then, the angles could be reduced to one, using the Gegenbauer polynomials technique [1]. Using this technique, the a_μ^{LbL} can be averaged over the direction of the muon in space such that

$$< \cdots > = \frac{1}{2\pi^2} \int d\Omega(\hat{p}) \quad . \tag{5.13}$$

25

To do so, one defines $(4) \equiv (P + P_1)^2 + m_\mu^2$ and $(5) \equiv (P - P_2)^2 + m_\mu^2$ with $P^2 = -m_\mu^2$, to find [1]

$$
< \frac{1}{(4)} \frac{1}{(5)} > = \frac{1}{m_\mu^2 R_{12}} \arctan\left(\frac{zx}{1 - zt}\right)
$$

$$
< (P.P_1)\frac{1}{(5)} > = (P_1 \cdot P_2)\frac{(1 - R_{m2})^2}{8m_\mu^2}
$$

$$
< (P.P_2)\frac{1}{(4)} > = (P_1 \cdot P_2)\frac{(1 - R_{m1})^2}{8m_\mu^2}
$$

$$
< \frac{1}{(4)} > = -\frac{(1 - R_{m1})}{2m_\mu^2}
$$

$$
< \frac{1}{(5)} > = -\frac{(1 - R_{m2})}{2m_\mu^2} \ , \tag{5.14}
$$

where

$$
R_{mi} = \sqrt{1 + \frac{4m_\mu^2}{Q_i^2}} \tag{5.15}
$$

and

$$
z = \frac{P_1 P_2}{4m_\mu^2}(1 - R_{m1})(1 - R_{m2}) \ . \tag{5.16}
$$

Also, $t = \cos\theta$ and θ is the azimuthal angle between the momenta P_1 and P_2.

The integral (5.10) reduces to a three dimensional integral

$$
a_\mu^{LbL} = -\frac{2\alpha^3}{3\pi^2} \int_0^\infty dP_1 dP_2 \int_{-1}^{+1} dt \sqrt{1 - t^2} P_1^3 P_2^3 \left[\frac{F_1 I_1(P_1, P_2, t)}{(P_2^2 + m_\pi^2)} + \frac{F_2 I_2(P_1, P_2, t)}{(Q^2 + m_\pi^2)} \right] \ , \tag{5.17}
$$

where

$$
\begin{aligned}
I_1(P_1, P_2, t) =\ & 1/(P_1^2 P_2^2 Q^2)\bigg[X(P_1, P_2, t)\Big(8Q^2(P_1 \cdot P_2) - 2P_2^2(P_2^4/m_\mu^2 - 2P_2^2) \\
& -\ 2P_2^2 Q^2(2 - P_2^2/m_\mu^2 + 2(P_1 \cdot P_2)/m_\mu^2) + 4P_1^4 \\
& -\ 4P_1^2 Q^2 - 2P_1^2 P_2^2(4 + P_1^2/m_\mu^2 - 2P_2^2/m_\mu^2) + 2/m_\mu^2\Big) \\
& -\ 2Q^2(1 + (1 - R_{m1})(P_1 \cdot P_2)/m_\mu^2) + P_2^2(2 - (1 - R_{m1})P_2^2/m_\mu^2) \\
& +\ P_2^2 Q^2(1 - R_{m1})/m_\mu^2 + P_1^2(2 + (1 - R_{m1})^2(P_1 \cdot P_2)/m_\mu^2) \\
& +\ 3P_1^2 P_2^2(1 - R_{m1})/m_\mu^2 \bigg] \ , \tag{5.18}
\end{aligned}
$$

26

pion exchange contribution	$a_\mu \times 10^{10}$
Bijnens, Pallante and Prades [11]	5.6
Hayakawa and Kinoshita [13]	5.7
Knecht and Nyffeler [14]	5.8
Melnikov and Vainshtein [16]	7.65

Table 2: Results of different calculations for the pion exchange contribution to a_μ.

$$
\begin{aligned}
I_2(P_1, P_2, t) \;=\; & 1/(P_1^2 P_2^2 Q^2)\Bigg[X(P_1, P_2, t)\Big(4Q^2(P_1 \cdot P_2) + 2P_2^4 - 2P_2^2 Q^2 + 2P_1^4 \\
& - 2P_1^2 Q^2 - 4P_1^2 P_2^2 - 4/m_\mu^2\Big) - 2Q^2 - 3P_2^2 Q^2 (1 - R_{m2})/(2m_\mu^2) \\
& - 3P_1^2 Q^2 (1 - R_{m1})/(2m_\mu^2) + P_2^2(2 + 3(1 - R_{m2})P_2^2/(2m_\mu^2)) \\
& + (1 - R_{m2})^2(P_1 \cdot P_2)/(2m_\mu^2) + P_1^2(2 + 3(1 - R_{m1})P_1^2/(2m_\mu^2)) \\
& + (1 - R_{m1})^2(P_1 \cdot P_2)/(2m_\mu^2) - P_1^2 P_2^2(2 - R_{m1} - R_{m2})/(2m_\mu^2)\Bigg] \quad (5.19)
\end{aligned}
$$

The auxiliary function is

$$
X(P_1, p_2, t) = \frac{1}{p_1 p_2 x} \arctan\left(\frac{zx}{1 - zt}\right) \quad . \tag{5.20}
$$

So, using this technique, one manages to reduce the eight dimensional integral (5.10) to a three dimensional one. Instead of t one can also use $Q^2 = P_1^2 + P_2^2 + 2P_1 P_2$ as variable. Results for the different calculations for the pion exchange are shown in Table 2. These correspond to different choices of $\mathcal{F}_{\pi^{0\star}\gamma^\star\gamma}(q^2, p_1^2, p_2^2)$.

5.2.2 Bare pion loop

What was described above for the pion exchange case we now extend to the charged pion loop case which is the topic of this work. This is the contribution of scalar QED which is renormalizable. For the pion loop after evaluating the four–point function in (5.4) all functions in (5.7) are nonzero.

The contribution of the hadronic light by light scattering arises at the order of $(\alpha/\pi)^3$. This includes box diagrams shown in Figure 16, triangle diagrams in Figure 17 and bulb diagrams, shown in Figure 18. These diagrams, along with their charge conjugates, add up to 21.

Among the contributions to the four point function denoted in the relation (5.7), the $\Pi^{ijkm}(p_1, p_2, p_3)$ ones originate only from the box diagrams of Figure 16, the $\Pi^{ijk}(p_1, p_2, p_3)$ ones can originate both from the box and triangle diagrams and the $\Pi^i(p_1, p_2, p_3)$ functions come only from the bulb diagrams. One needs to find these functions, take their derivative
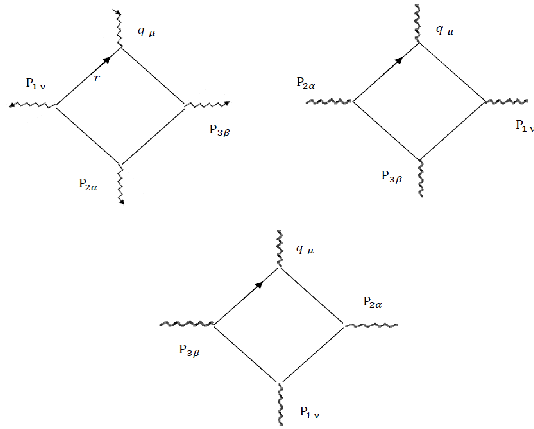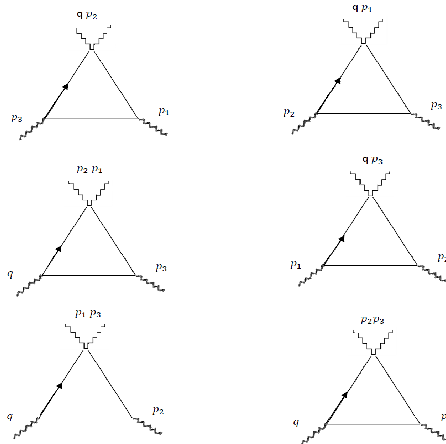
Figure 16: The box diagram contribution to the a_μ HLL.
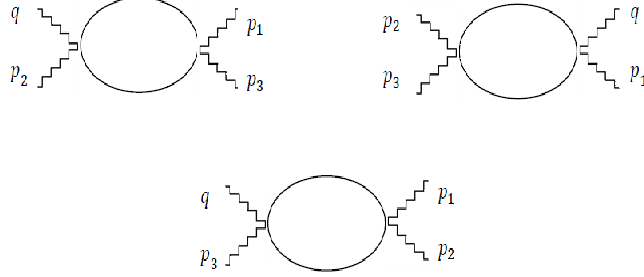

Figure 17: The triangle diagram contribution to the a_μ HLL.

Figure 18: The bulb diagram contribution to the a_μ HLL.

with respect to p_3, set $p_3 = 0$ and plug into the relation (5.3). To do so, we have used the code FORM.

Let us first illustrate the procedure with the corresponding four point function for the first diagram of the Figure 16. This diagram gives

$$\Pi_{\mu\nu\alpha\beta} =$$
$$\frac{1}{i} \int \frac{d^d r}{(2\pi)^d} \frac{i^4 \times i^4}{(r^2 - m^2)((r + p_1)^2 - m^2)((r + p_1 + p_2)^2 - m^2)((r + p_1 + p_2 + p_3)^2 - m^2)}$$
$$\times (2r + p_1 + p_2 + p_3)_\mu (2r + p_1)_\nu (2r + 2p_1 + p_2)_\alpha (2r + 2p_1 + 2p_2 + p_3)_\beta \ . \tag{5.21}$$

Using the Feynman parametrization method

$$\frac{1}{abcd} = 6 \int_0^1 dx \int_0^{1-x} dy \int_0^{1-x-y} dz \frac{1}{[a(1 - x - y - z) + bx + cy + dz]^4} \ , \tag{5.22}$$

one obtains

$$\Pi_{\mu\nu\alpha\beta} = \frac{6}{i} \int \frac{d^4 \tilde{r}}{(2\pi)^4} \int_0^1 dx \int_0^{1-x} dy \int_0^{1-x-y} dz \frac{1}{\tilde{r}^2 - \tilde{m}^2}$$
$$(2r + p_1 + p_2 + p_3)_\mu (2r + p_1)_\nu (2r + 2p_1 + p_2)_\alpha (2r + 2p_1 + 2p_2 + p_3)_\beta \ , \tag{5.23}$$

with

$$\tilde{m}^2 = m^2 + \left((x + y + z)p_1 + (y + z)p_2 + zp_3\right)^2 - xp_1^2 - y(p_1 + p_2)^2 - z(p_1 + p_2 + p_3)^2$$
$$\tilde{r} = r + (x + y + z)p_1 + (y + z)p_2 + zp_3 \ . \tag{5.24}$$

29

To deal with the integrals we have used the relations

$$\int \frac{d^d r}{(2\pi)^d} \tilde{r}_\mu \tilde{r}_\nu \tilde{r}_\alpha \tilde{r}_\beta f(\tilde{r}^2) = \int \frac{d^d r}{(2\pi)^d} \frac{1}{d(d+2)} \tilde{r}^4 (g_{\mu\nu} g_{\alpha\beta} + g_{\mu\beta} g_{\alpha\nu} + g_{\nu\beta} g_{\alpha\mu}) f(\tilde{r}^2)$$

$$\int \frac{d^d r}{(2\pi)^d} \tilde{r}_\mu \tilde{r}_\nu f(\tilde{r}^2) = \int \frac{d^d r}{(2\pi)^d} \frac{1}{d} \tilde{r}^2 g_{\mu\nu} f(\tilde{r}^2) \ , \tag{5.25}$$

and that integrals with odd powers in the numerator vanish. The remaining integrals to be done are

$$\frac{1}{d(d+2)} \frac{1}{i} \int \frac{d^d \tilde{r}}{(2\pi)^d} \frac{\tilde{r}^4}{(\tilde{r}^2 - \tilde{m}^2)^4} = \frac{1}{d(d+2)i} \int \frac{dr^d}{(2\pi)^d}$$

$$\left[\frac{1}{(\tilde{r}^2 - \tilde{m}^2)^2} + \frac{2\tilde{m}^2}{(\tilde{r}^2 - \tilde{m}^2)^3} + \frac{\tilde{m}^4}{(\tilde{r}^2 - \tilde{m}^2)^4} \right]$$

$$= \frac{1}{24} \frac{1}{16\pi^2} [\frac{1}{\tilde{\varepsilon}} + \frac{5}{6} - 1 - ln\frac{\tilde{m}^2}{\mu^2} - 1 + \frac{1}{6}]$$

$$= \frac{1}{24} \frac{1}{16\pi^2} [\frac{1}{\tilde{\varepsilon}} - 1 - ln\frac{\tilde{m}^2}{\mu^2}] \ , \tag{5.26}$$

$$\frac{1}{d} \frac{1}{i} \int \frac{d^d \tilde{r}}{(2\pi)^d} \frac{\tilde{r}^2}{(\tilde{r}^2 - \tilde{m}^2)^4} = \frac{1}{di} \int \frac{dr^d}{(2\pi)^d}$$

$$\left[\frac{1}{(\tilde{r}^2 - \tilde{m}^2)^3} + \frac{\tilde{m}^2}{(\tilde{r}^2 - \tilde{m}^2)^4} \right]$$

$$= \frac{1}{4} \frac{1}{16\pi^2} \left(\frac{-1}{2\tilde{m}^2} + \frac{1}{6\tilde{m}^2} \right) = \frac{1}{16\pi^2} \frac{-1}{12\tilde{m}^2} \tag{5.27}$$

and

$$\frac{1}{i} \int \frac{d^d \tilde{r}}{(2\pi)^d} \frac{1}{(\tilde{r}^2 - \tilde{m}^2)^4} = \frac{1}{16\pi^2} \frac{1}{6} \frac{1}{\tilde{m}^4} \ . \tag{5.28}$$

where μ is the subtraction scale of the problem at hand, $d = 4 - 2\varepsilon$, $1/\tilde{\varepsilon} = 1/(\varepsilon - ln 4\pi + \gamma + 1)$, γ is the Euler-Mascheroni constant and ε creeps in from the dimensional regularization. The expressions for the integral

$$\int \frac{d^d \tilde{r}}{(2\pi)^d} \frac{1}{(\tilde{r}^2 - \tilde{m}^2)^4} \tag{5.29}$$

can be found in [5]. Then, one evaluates the derivative $\partial \Pi_{\mu\nu\alpha\beta}/\partial p_3$, which means deriving $\tilde{m}^2$ or occurrences of p_3 in the numerator, and put $p_3 = 0$ to find the relevant function to be integrated over. A similar procedure is done for the other box diagrams.

30

For the first triangle diagram shown in Figure 17 the four point function reads

$$
\begin{aligned}
\Pi_{\mu\nu\alpha\beta} \;=\; \\
\frac{1}{i}\;\int \frac{d^4r}{(2\pi)^4}\,\frac{i^3 \times i^3}{(r^2-m^2)((r+p_2)^2-m^2)((r+p_2+p_3)^2-m^2)} \\
\times\; g_{\mu\nu}\,(2r+p_2)_\alpha(2r+2p_2+p_3)_\beta \;,
\end{aligned}
\tag{5.30}
$$

which can be parameterized using

$$
\frac{1}{abc} = 6\int_0^1 dx \int_0^{1-x} dy\,\frac{1}{[a(1-x-y)+bx+cy]^3} \;,
\tag{5.31}
$$

to give

$$
\Pi_{\mu\nu\alpha\beta} = \frac{1}{i}\int \frac{d^4\tilde{r}}{(2\pi)^4}\,\frac{i^3\times i^3}{\tilde{r}^2-\tilde{m}^2}g_{\mu\nu}(2r+p_2)_\alpha(2r+2p_2+p_3)_\beta \;,
$$

with

$$
\begin{aligned}
\tilde{m}^2 &=\; m^2 + \Big((x+y)p_2+yp_3\Big)^2 - xp_2^2 - y(p_2+p_3)^2 \\
\tilde{r} &=\; r + (x+y)p_2 + yp_3 \;.
\end{aligned}
\tag{5.32}
$$

Then using again (5.25) and

$$
\begin{aligned}
\frac{1}{d}\frac{1}{i}\int \frac{d^d\tilde{r}}{(2\pi)^d}\,\frac{\tilde{r}^2}{(\tilde{r}^2-\tilde{m}^2)^3} \;=\; \\
=\; \frac{1}{4}\frac{1}{16\pi^2}\left[\frac{1}{\tilde{\varepsilon}}+\frac{1}{2}-1-ln\frac{\tilde{m}^2}{\mu^2}-\frac{1}{2}\right] \\
=\; \frac{1}{4}\frac{1}{16\pi^2}\left[\frac{1}{\tilde{\varepsilon}}-1-ln\frac{\tilde{m}^2}{\mu^2}\right] \;,
\end{aligned}
\tag{5.33}
$$

one gets

$$
\frac{1}{i}\int \frac{d^d\tilde{r}}{(2\pi)^d}\,\frac{1}{(\tilde{r}^2-\tilde{m}^2)^3} = \frac{1}{4}\frac{1}{16\pi^2}\frac{-1}{2\tilde{m}^2} \;.
\tag{5.34}
$$

And finally, for the first bulb diagram of Figure 18 one has

$$
\begin{aligned}
\Pi_{\mu\nu\alpha\beta} \;=\; \\
\frac{1}{i}\;\int \frac{d^4r}{(2\pi)^4}\,\frac{i^2\times i^2}{(r^2-m^2)((r+p_2+p_3)^2-m^2)} \\
\times 2\,g_{\mu\nu}\,2g_{\alpha\beta} = \frac{1}{i}\int \frac{d^4\tilde{r}}{(2\pi)^4}\int_0^1 dx\,\frac{1}{(\tilde{r}^2-\tilde{m}^2)^2}\times 4g_{\mu\nu}g_{\alpha\beta} \\
=\; 4\frac{1}{16\pi^2}\left[\frac{1}{\tilde{\varepsilon}}-1-ln\frac{\tilde{m}^2}{\mu}\right]g_{\mu\nu}g_{\alpha\beta} \;,
\end{aligned}
\tag{5.35}
$$

31

with

$$\tilde{r} = r + x(p_2 + p_3) \tag{5.36}$$

and

$$\tilde{m}^2 = m_p^2 + x(x-1)(p_2 + p_3) \ . \tag{5.37}$$

It is important to notice that the divergent parts of each diagrams, when added up, cancel each other and the remaining part which contributes to the a_μ is finite. As a consequence, all $ln\mu^2$ dependent terms above disappear miraculously.

After doing the above integrations, depending on the type of the diagram, we apply the Gegenbauer polynomial method to perform five of the integrations in (5.6) similar to the steps that led to (5.17). The final formula is rather long and is not presented here. Besides the P_1, P_2, t or P_1, P_2, Q integration one is always left with one, two or three Feynman parameters that should also be integrated over. One can always shift the parameters in the case of box and triangle diagrams so that, the denominator is independent of one of them, and it could be analytically integrated out, reducing the size of the expressions considerably. It turns out that the different $\tilde{m}^2$ for the different box diagrams can all be brought in the same form as well reducing the size of the expressions considerably. The final integral to be done is a five or four dimensional integral, which we have dealt with using the Monte Carlo routine VEGAS.

5.2.3   HLS

When trying the same procedure for the HLS case, we can reuse a lot of the previous subsection since the vertices are related by (4.3) and (4.4). One should be careful since, terms including $p.\tilde{r}$ will also appear in the numerator. For example, for the Figure 5, the four point function of the HLS is

$$\Pi_{\mu\nu\alpha\beta} =$$
$$\frac{1}{i}\int \frac{d^4r}{(2\pi)^4} \frac{i^4 \times i^4}{(r^2 - m^2)((r+p_1)^2 - m^2)((r+p_1+p_2)^2 - m^2)((r+p_1+p_2+p_3)^2 - m^2)}$$
$$\times(2r + p_1 + p_2 + p_3)_\mu \left(g_{\mu\bar{\mu}} - \frac{q^2 g_{\mu\bar{\mu}} - q_\mu q_{\bar{\mu}}}{q^2 - m_\rho^2} \right)$$
$$(2r + p_1)_\nu \left(g_{\nu\bar{\nu}} - \frac{p_1^2 g_{\nu\bar{\nu}} - p_{1\nu} p_{1\bar{\nu}}}{p_1^2 - m_\rho^2} \right)$$
$$(2r + 2p_1 + p_2)_\alpha \left(g_{\alpha\bar{\alpha}} - \frac{p_2^2 g_{\alpha\bar{\alpha}} - p_{2\alpha} p_{2\bar{\alpha}}}{p_2^2 - m_\rho^2} \right)$$
$$(2r + 2p_1 + 2p_2 + p_3)_\beta \left(g_{\beta\bar{\beta}} - \frac{p_3^2 g_{\beta\bar{\beta}} - p_{3\beta} p_{3\bar{\beta}}}{p_3^2 - m_\rho^2} \right) \ . \tag{5.38}$$

The four point function of the first diagram of Figure 17 becomes

$$
\begin{aligned}
\Pi_{\mu\nu\alpha\beta} \quad = \\
\frac{1}{i} \int \frac{d^4r}{(2\pi)^4} \frac{i^3 \times i^3}{(r^2 - m^2)((r+p_2)^2 - m^2)((r+p_2+p_3)^2 - m^2)} \\
\times \; g_{\mu\nu} 2\left(g_{\mu\bar{\mu}}g_{\nu\bar{\nu}} + g_{\mu\bar{\mu}}\frac{a}{2}\frac{p_1^2 g_{\nu\bar{\nu}} - p_{1\bar{\nu}}p_{1\nu}}{m_\rho^2 - p_1^2} + g_{\nu\bar{\nu}}\frac{a}{2}\frac{q^2 g_{\mu\bar{\mu}} - q_{\bar{\mu}}q_{\mu}}{m_\rho^2 - q^2}\right) \\
(2r \; + \; p_2)_\alpha \left(g_{\alpha\bar{\alpha}} - \frac{p_2^2 g_{\alpha\bar{\alpha}} - p_{2\alpha}p_{2\bar{\alpha}}}{p_2^2 - m_\rho^2}\right) \\
(2r \; + \; 2p_2 + p_3)_\beta \left(g_{\beta\bar{\beta}} - \frac{p_3^2 g_{\beta\bar{\beta}} - p_{3\beta}p_{3\bar{\beta}}}{p_3^2 - m_\rho^2}\right) \quad\quad\quad\quad\quad (5.39)
\end{aligned}
$$

and the four point function corresponding to the first bulb of Figure 18 is

$$
\begin{aligned}
\Pi_{\mu\nu\alpha\beta} \quad = \\
\frac{1}{i} \int \frac{d^4r}{(2\pi)^4} \frac{i^2 \times i^2}{(r^2 - m^2)((r+p_2+p_3)^2 - m^2)} \\
\times 2g_{\mu\nu} 2g_{\alpha\beta}\left(g_{\mu\bar{\mu}}g_{\nu\bar{\nu}} + g_{\mu\bar{\mu}}\frac{a}{2}\frac{p_1^2 g_{\nu\bar{\nu}} - p_{1\bar{\nu}}p_{1\nu}}{m_\rho^2 - p_1^2} + g_{\nu\bar{\nu}}\frac{a}{2}\frac{q^2 g_{\mu\bar{\mu}} - q_{\bar{\mu}}q_{\mu}}{m_\rho^2 - q^2}\right) \\
\left(g_{\beta\bar{\beta}}g_{\alpha\bar{\alpha}} + g_{\beta\bar{\beta}}\frac{a}{2}\frac{p2^2 g_{\alpha\bar{\alpha}} - p_{2\bar{\alpha}}p_{2\alpha}}{m_\rho^2 - p_2^2} + g_{\alpha\bar{\alpha}}\frac{a}{2}\frac{p_3^2 g_{\beta\bar{\beta}} - p_{3\beta}p_{3\beta}}{m_\rho^2 - p_3^2}\right) \; . \quad (5.40)
\end{aligned}
$$

To deal with terms like $p \cdot \tilde{r}$ one can use the relations (5.26), (5.27) and (5.28), but some of the $\tilde{r}$s couple to p.

Furthermore, as for the infinities in the HLS approach, they only cancel out after taking the derivative with respect to p_3 and setting $p_3 = 0$. The HLS is not a renormalizable theory, and thus the result could have been divergent but surprisingly, the contribution to a_μ is finite.

5.2.4   Full VMD

As it was described in Sec. 4 in the full VMD, $\gamma\pi\pi$ vertex is multiplied with (4.5). However, how it deals with the need of being chiral and gauge invariant, that the naive VMD model does not meet. In fact, it could be shown that covering the photon legs with vector mesons when using (4.5), because of the Ward identities in 5.8, always the second term in this expression cancels and the result is just like multiplying each photon leg with $m_\rho^2/(m_\rho^2 - q^2)$, and this is fully invariant under above mentioned symmetries.

Now let us illustrate how the four point function changes in this model. Again us-

ing (4.5), (4.5) and (5.21) one finds

$$\Pi_{\mu\nu\alpha\beta} =$$
$$\frac{1}{i}\int \frac{d^4r}{(2\pi)^4} \frac{i^4 \times i^4}{(r^2 - m^2)((r + p_1)^2 - m^2)((r + p_1 + p_2)^2 - m^2)((r + p_1 + p_2 + p_3)^2 - m^2)}$$
$$\times (2r + p_1 + p_2 + p_3)_\mu \left(\frac{g_{\mu\bar\mu}m_\rho^2 - q_\mu q_{\bar\mu}}{m_\rho^2 - q^2} \right)$$
$$(2r + p_1)_\nu \left(\frac{g_{\bar\nu\nu}m_\rho^2 - p_{1\nu}p_{1\bar\nu}}{m_\rho^2 - p_1^2} \right)$$
$$(2r + 2p_1 + p_2)_\alpha \left(\frac{g_{\alpha\bar\alpha}m_\rho^2 - P_{2\alpha}p_{2\bar\alpha}}{m_\rho^2 - p_2^2} \right)$$
$$(2r + 2p_1 + 2p_2 + p_3)_\beta \left(\frac{g_{\beta\bar\beta}m_\rho^2 - p_{3\beta}p_{3\bar\beta}}{m_\rho^2 - p_3^2} \right) \quad . \tag{5.41}$$

For the first triangle diagram of Figure 17 the four–point function writes

$$\Pi_{\mu\nu\alpha\beta} =$$
$$\frac{1}{i}\int \frac{d^4r}{(2\pi)^4} \frac{i^3 \times i^3}{(r^2 - m^2)((r + p_2)^2 - m^2)((r + p_2 + p_3)^2 - m^2)}$$
$$\times g_{\mu\nu} 2\left(\frac{m_\rho^2 g_{\nu\bar\nu} - p_{1\bar\nu}p_{1\nu}}{m_\rho^2 - p_1^2} \frac{m_\rho^2 g_{\mu\bar\mu} - q_{\bar\mu}q_\mu}{m_\rho^2 - q^2} \right)$$
$$(2r + p_2)_\alpha \left(\frac{g_{\alpha\bar\alpha}m_\rho^2 - p_{2\alpha}p_{2\bar\alpha}}{m_\rho^2 - p_2^2} \right)$$
$$(2r + 2p_2 + p_3)_\beta \left(\frac{g_{\beta\bar\beta}m_\rho^2 - p_{3\beta}p_{3\bar\beta}}{m_\rho^2 - p_3^2} \right) \tag{5.42}$$

and for the first bulb diagram of Figure 18 one has

$$\Pi_{\mu\nu\alpha\beta} =$$
$$\frac{1}{i}\int \frac{d^4r}{(2\pi)^4} \frac{i^2 \times i^2}{(r^2 - m^2)((r + p_2 + p_3)^2 - m^2)}$$
$$\times 2g_{\mu\nu} 2g_{\alpha\beta} \left(\frac{m_\rho^2 g_{\nu\bar\nu} - p_{1\bar\nu}p_{1\nu}}{m_\rho^2 - p_1^2} \frac{m_\rho^2 g_{\mu\bar\mu} - q_{\bar\mu}q_\mu}{m_\rho^2 - q^2} \right)$$
$$\times \left(\frac{m_\rho^2 g_{\alpha\bar\alpha} - p_{2\bar\alpha}p_{2\alpha}}{m_\rho^2 - p_2^2} \frac{m_\rho^2 g_{\beta\bar\beta} - p_{3\bar\beta}p_{3\beta}}{m_\rho^2 - p_3^2} \right) \quad . \tag{5.43}$$

5.2.5 L_9 and L_{10}

Since Ref. [25] argued that order p^4 effects might be important, we have also calculated the contributions of L_9 and L_{10} to this order. Using the previous results, the four point

function of the Figure 5, taking into account the L_9 and L_{10} corrections, takes the form

$$\Pi_{\mu\nu\alpha\beta} =$$

$$\frac{1}{i} \int \frac{d^4r}{(2\pi)^4} \frac{i^4 \times i^4}{(r^2 - m^2)((r + p_1)^2 - m^2)((r + p_1 + p_2)^2 - m^2)((r + p_1 + p_2 + p_3)^2 - m^2)}$$

$$\times (2r + p_1 + p_2 + p_3)_\mu \left(g_{\mu\bar\mu} + L_9(q^2 g_{\mu\bar\mu} - q_\mu q_{\bar\mu}) \right)$$

$$(2r + p_1)_\nu \left(g_{\nu\bar\nu} + L_9(p_1^2 g_{\nu\bar\nu} - p_{1\nu} p_{1\bar\nu}) \right)$$

$$(2r + 2p_1 + p_2)_\alpha \left(g_{\alpha\bar\alpha} + L_9(p_2^2 g_{\alpha\bar\alpha} - p_{2\alpha} p_{2\bar\alpha}) \right)$$

$$(2r + 2p_1 + 2p_2 + p_3)_\beta \left(g_{\beta\bar\beta} + L_9(p_3^2 g_{\beta\bar\beta} - p_{3\beta} p_{3\bar\beta}) \right) \ . \tag{5.44}$$

The same function for the first triangle diagram of Figure 17 writes

$$\Pi_{\mu\nu\alpha\beta} =$$

$$\frac{1}{i} \int \frac{d^4r}{(2\pi)^4} \frac{i^3 \times i^3}{(r^2 - m^2)((r + p_2)^2 - m^2)((r + p_2 + p_3)^2 - m^2)}$$

$$\times g_{\mu\nu} \left(g_{\mu\bar\mu} g_{\nu\bar\nu} + g_{\mu\bar\mu} L_9 \left(p_1^2 g_{\nu\bar\nu} - p_{1\bar\nu} p_{1\nu} \right) + g_{\nu\bar\nu} L_9 \left(q^2 g_{\mu\bar\mu} - q_{\bar\mu} q_\mu \right) \right.$$

$$\left. + (L_9 + L_{10}) \left(q \cdot p_1 g_{\mu\bar\mu} g_{\nu\bar\nu} - g_{\mu\nu} p_{1\bar\mu} q_{\bar\nu} \right) \right)$$

$$(2r + p_2)_\alpha \left(g_{\alpha\bar\alpha} + L_9(p_2^2 g_{\alpha\bar\alpha} - p_{2\alpha} p_{2\bar\alpha}) \right)$$

$$(2r + 2p_2 + p_3)_\beta \left(g_{\beta\bar\beta} + L_9(p_3^2 g_{\beta\bar\beta} - p_{3\beta} p_{3\bar\beta}) \right) \tag{5.45}$$

and the four point function of the first bulb diagram of the Figure 18 is

$$\Pi_{\mu\nu\alpha\beta} =$$

$$\frac{1}{i} \int \frac{d^4r}{(2\pi)^4} \frac{i^2 \times i^2}{(r^2 - m^2)((r + p_2 + p_3)^2 - m^2)}$$

$$\times 2g_{\mu\nu} 2g_{\alpha\beta} \left(g_{\mu\bar\mu} g_{\nu\bar\nu} + g_{\mu\bar\mu} L_9 \left(p_1^2 g_{\nu\bar\nu} - p_{1\bar\nu} p_{1\nu} \right) + g_{\nu\bar\nu} L_9 \left(q^2 g_{\mu\bar\mu} - q_{\bar\mu} q_\mu \right) \right.$$

$$\left. + (L_9 + L_{10}) \left(q \cdot p_1 g_{\mu\bar\mu} g_{\nu\bar\nu} - g_{\mu\nu} p_{1\bar\mu} q_{\bar\nu} \right) \right)$$

$$\left(g_{\alpha\bar\alpha} g_{\beta\bar\beta} + g_{\alpha\bar\alpha} L_9 \left(p_3^2 g_{\beta\bar\beta} - p_{3\bar\beta} p_{3\beta} \right) + g_{\beta\bar\beta} L_9 \left(p_2^2 g_{\alpha\bar\alpha} - p_{2\bar\alpha} p_{2\alpha} \right) \right.$$

$$\left. + (L_9 + L_{10}) \left(p_2 \cdot p_3 g_{\alpha\bar\alpha} g_{\beta\bar\beta} - g_{\alpha\beta} p_{3\bar\alpha} p_{2\bar\beta} \right) \right) \ . \tag{5.46}$$

Methods for doing the integrals are the same as of the HLS part. Furthermore, in this case the $\Pi^{\mu\nu\alpha\beta}$ are finite whereas, contribution to a_μ are not finite.

Cut-off	$10^{10}a_\mu$				
GeV	bare	VMD	HLS $a=2$	L_9, L_{10}	HLS $a=1$
0.5	$-1.71(7)$	$-1.16(3)$	$-1.05(1)$	$-1.64(1)$	$-1.35(1)$
0.6	$-2.03(8)$	$-1.41(4)$	$-1.15(1)$	$-1.80(1)$	$-1.59(1)$
0.7	$-2.41(9)$	$-1.46(4)$	$-1.17(1)$	$-1.85(1)$	$-1.76(1)$
0.8	$-2.64(9)$	$-1.57(6)$	$-1.16(1)$	$-1.79(1)$	$-1.88(1)$
1.0	$-2.97(12)$	$-1.59(15)$	$-1.07(1)$	$-1.53(1)$	$-2.03(1)$
2.0	$-3.82(18)$	$-1.70(7)$	$-0.68(1)$	$+1.15(1)$	$-2.16(1)$
4.0	$-4.12(18)$	$-1.66(6)$	$-0.50(1)$	$+6.18(1)$	$-2.14(1)$

Table 3: Results of different calculations for the pion loop.

6 Relevant Momentum Regions for the pion Loop Contribution.

6.1 Dependence on the photon cut–off Λ

Up to this point, the process needed to be taken to calculate the a_μ for each approach has been described. It is now relevant to consider the way a_μ behaves under change of momenta. In fact, one expects that since the HLS model and the ChPT in higher orders are non renormalizable, it should be somehow visible through the a_μ as well. Furthermore, after all one of the main goals of the present work has been to deal with differences of the VMD and HLS model. One can also expect that the differences should somehow reveal themselves via these considerations. To see how, we have calculated different values of a_μ for different cut–offs so that $P_1 < \Lambda, P_2 < \Lambda, Q < \Lambda$ and results are shown in Table3.

As can be seen, the HLS and the VMD have the same behavior in low momentum region however, for higher momenta, HLS starts to behave oddly. Meanwhile, the L_9, L_{10} behavior for higher momenta is as expected due to the non–renormalizability of ChPT in order p^4.

6.2 Anatomy of the relevant momentum regions for the pion Loop Contribution.

But, as it has been discussed in the Ref. [6], one can also investigate how different regions of momentum, contribute differently to the HLL contribution to the a_μ. The technique is the same with calculating the whole value of a_μ but this time, instead of taking the integral over all variables, one leaves $P_1^2 = -p_1^2$, $P_2^2 = -p_2^2$ and $Q^2 = -q^2$ unintegrated.
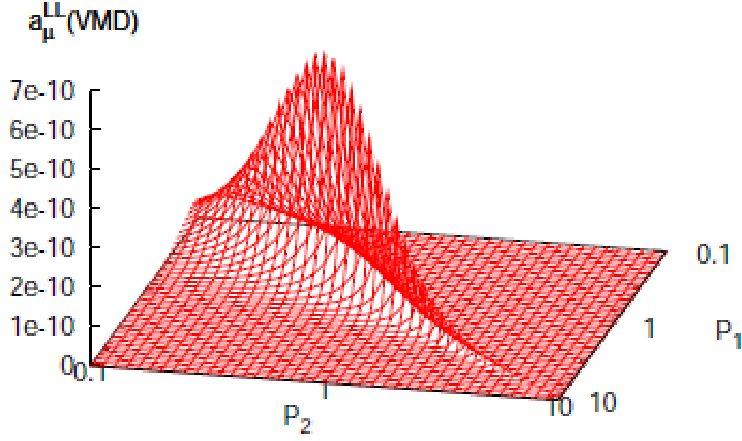
Figure 19: a_μ^{LL} of the Eq. (19) as a function of P_1 and P_2 for the VMD choice for the pion exchange. a_μ is directly related to the volume under the surface. Figure from [6].

Mathematically we write

$$
\begin{aligned}
a_\mu &= \int dl_1 dl_2 a_\mu^{LL}(l_1, l_2) \\
&= \int dl_1 dl_2 dl_q a_\mu^{LLQ}(l_1, l_2, l_q) \ ,
\end{aligned}
\tag{6.1}
$$

with $l_1 = log(P_1/GeV)$, $l_2 = log(P_2/GeV)$ and $l_q = log(Q/GeV)$. To see exactly how the momentum region above the 1 GeV contribute to the a_μ, it is better to use logarithmic scale as has been discussed in [6]. Also, the total amount of a_μ is proportional to the volume under the surface of each diagram. For example, as is shown in the Figure 19, the most important contribution of the pion exchange to the a_μ, via the VMD model, is coming from the low region of momenta, which is expected since, because of the usage of vector meson legs, the large momenta are strongly suppressed. Furthermore, the concentration is around the equal values of momenta P_1 and P_2. It should also be noticed that, the whole value of the a_μ is proportional to the volume under the surface, after integrating over the whole region of momenta. Also, as it is easier to deal with plots with positive values, $-a_\mu$ is drawn in the figures for the pion loop.

As can be seen from Figure 19, the momentum is concentrated along the line $P_1 = P_2$. Following the same lines as in [6], we have done the same calculation for the Bare, VMD, HLS and L_9, L_{10} approaches to the charged pion loop contribution to the a_μ and compared them. For each case we have shown the distribution of a_μ^{LLQ} versus P_1, Q and Q. Figures 20 and 21 belong to the bare pion loop case, where the peak is in the low momentum region but, a large part comes from the region above 1 GeV. I Figure 20 we also show the cases for $P_1 \neq P_2$. It is clear that the parts with P_1 significantly different from P_2 contribute less. In Figure 21 we show the case $P_1 = P_2$ alone.
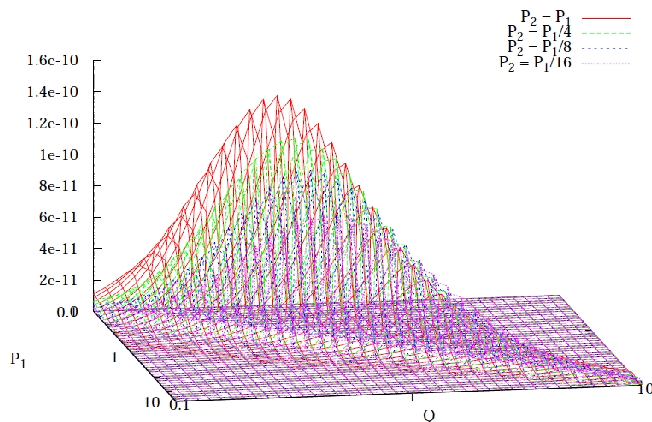
Figure 20: $-a_\mu^{LL}$ as a function of different ratios of P_1 and P_2 versus Q for the bare pion loop choice for. $-a_\mu$ is directly related to the volume under the surface.

Figures 22 shows the VMD case, which is obviously suppressed respect to the bare pion loop case, while the pick still lies in the low momentum region. Figure 23 compares the bare and the VMD cases.

Figures 24 and 25 belong to the HLS case for $a = 1$ and $a = 2$ respectively, where the second one should reproduce the VMD results. Here is where the surprise comes in and, as can be seen, the low momentum region peak follows with a dip at the high momentum region. The resulting graphes of HLS and VMD are co–plotted in Figure 26, in terms of $P_1 = P_2$ and Q. Conclusion to be drawn from this diagram is, in both approaches the main body of the contribution comes from the low momentum region and in the VMD case the large Q tail is larger. But, the large negative contribution to a_μ in the HLS side needs some justification. This finding gives a better insight into the nature of the difference which has led to such a dramatic variation between the full VMD and the HLS results. It should be mentioned that, as has been already noticed in the Ref. [10], the difference would stem from the lack of the $\rho\rho\pi\pi$ vertex in the HLS lagrangian. The case $a = 1$ in the HLS, which has a better higher energy behavior, makes the dip of the $a = 2$ case vanish.

Figures 27 and 28 show results of calculation for the L_9, L_{10} and $L_9 = -L_{10}$ cases and Figure 29 compares them. It should be mentioned that, as ChPT in the order p^4 is nonrenormalizable, the overall value of the a_μ in these cases are cutoff dependent. There is one specific property of the L_9 and L_{10} terms of the p^4 Lagrangian which we would like to emphasis that is, when one sets $L_{10} = -L_9$, the L_9 part contribution behaves like the HLS with $a = 2$ and the VMD part to order p^4. This could be seen in the Figures 30 and 31 and could be justified via relation (4.8) for the $\gamma\gamma\pi\pi$ vertex, when compared to the relation (4.4). Since, resorting to the fact that $L_9 \propto 1/m_\rho^2$ [23], relation (4.8) plays a similar role as the relation (4.4) does in the limit $L_{10} = -L_9$.
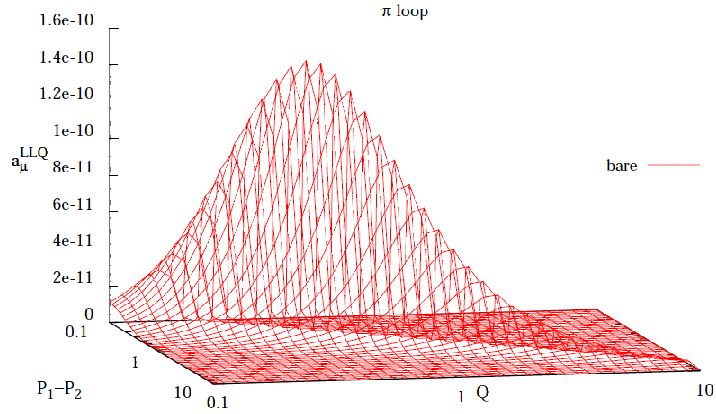
Figure 21: $-a_\mu^{LLQ}$ as a function of $P_1 = P_2$ and Q for the bare pion loop choice. $-a_\mu$ is directly related to the volume under the surface.
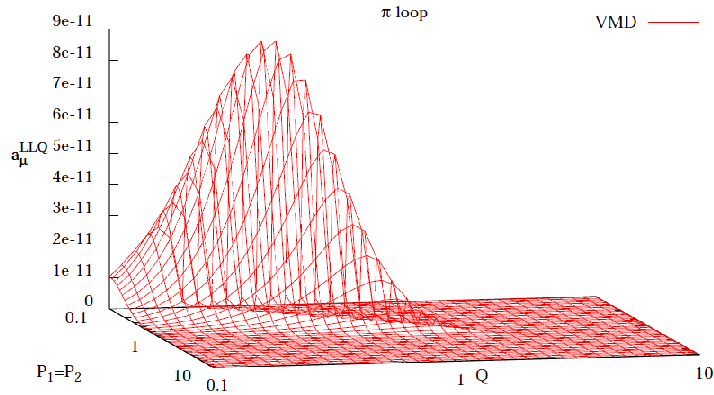

Figure 22: $-a_\mu^{LLQ}$ as a function of $P_1 = P_2$ and Q for the VMD choice. $-a_\mu$ is directly related to the volume under the surface.
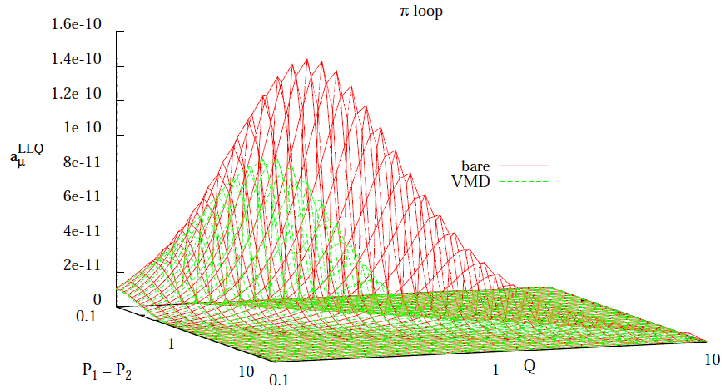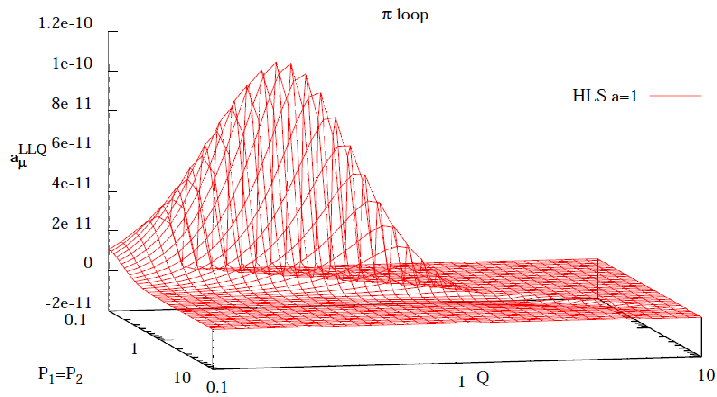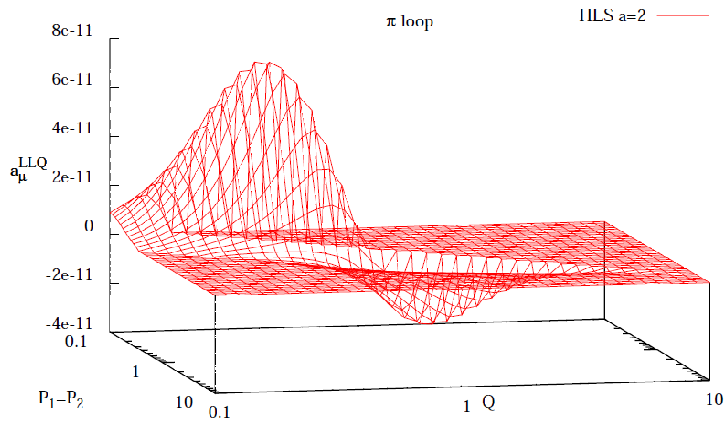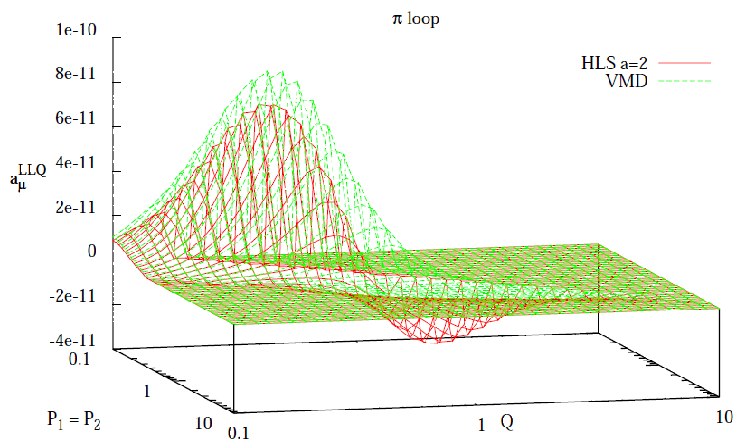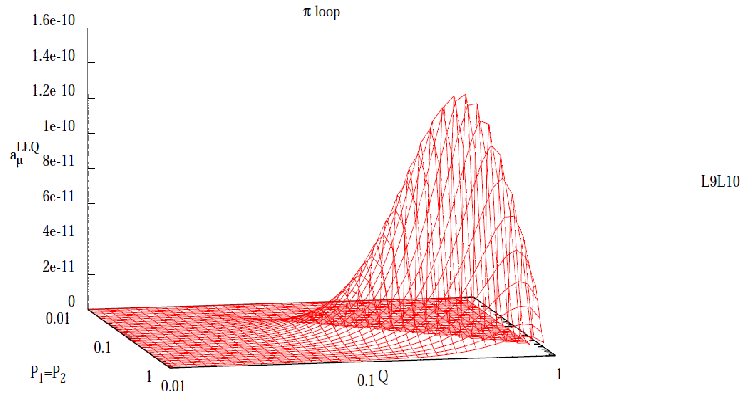
Figure 23: $-a_\mu^{LLQ}$ as a function of $P_1 = P_2$ and Q for the VMD and the bare pionloop choice. $-a_\mu$ is directly related to the volume under the surface.

Figure 24: $-a_\mu^{LLQ}$ as a function of $P_1 = P_2$ and Q for the HLS, $a = 1$ choice. $-a_\mu$ is directly related to the volume under the surface.
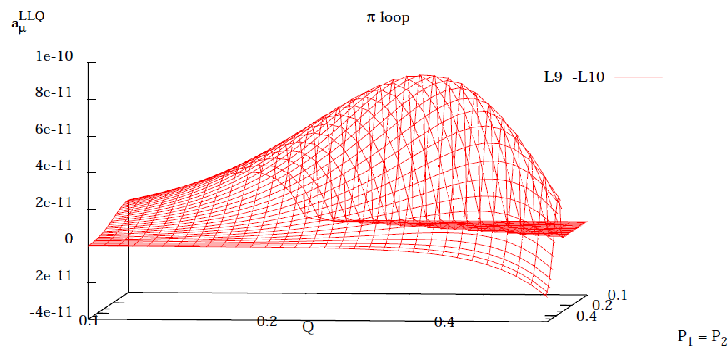
40

Figure 25: $-a_\mu^{LLQ}$ as a function of $P_1 = P_2$ and Q for the HLS, $a = 2$ choice. $-a_\mu$ is directly related to the volume under the surface.

Figure 26: $-a_\mu^{LLQ}$ of the Eq. (6.1) as a function of $P_1 = P_2$ and Q for the VMD and the HLS choices.

Figure 27: $-a_\mu^{LLQ}$ as a function of $P_1 = P_2$ and Q for the L_9, L_{10} choice. $-a_\mu$ is directly related to the volume under the surface.

Figure 28: $-a_\mu^{LLQ}$ of the Eq. (6.1) as a function of $P_1 = P_2$ and Q for the L_9 choice. $-a_\mu$ is directly related to the volume under the surface.
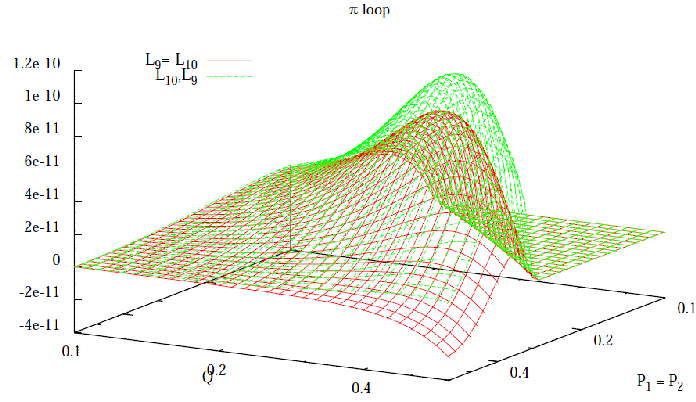
Figure 29: $-a_\mu^{LLQ}$ as a function of $P_1 = P_2$ and Q for the L_9 and L_9, L_{10} choice. $-a_\mu$ is directly related to the volume under the surface.
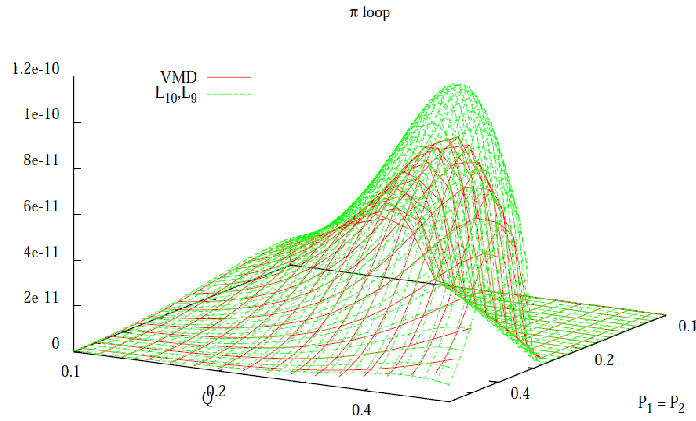

Figure 30: $-a_\mu^{LLQ}$ as a function of $P_1 = P_2$ and Q for the VMD and L_9, L_{10} choice. $-a_\mu$ is directly related to the volume under the surface.
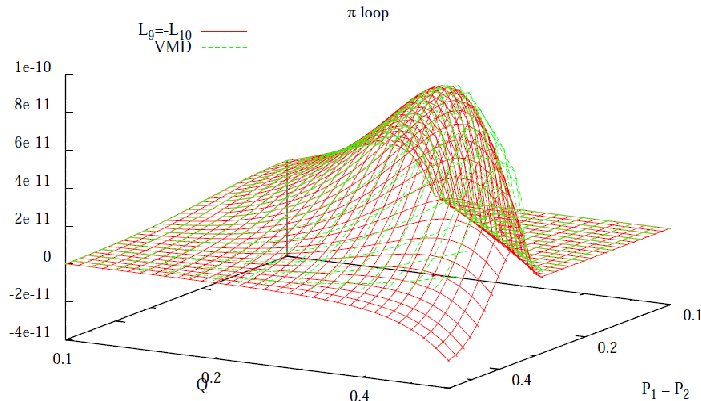
Figure 31: $-a_\mu^{LLQ}$ as a function of $P_1 = P_2$ and Q for the VMD and L_9 choice. $-a_\mu$ is directly related to the volume under the surface.

7 Conclusions and Prospects

In this work we have recalculated the previous results for the HLL pion loop contribution to the muon magnetic anomaly via the sQED, the VMD model and the HLS model and all results are in good agreement with the previous ones. To do so, we have extended the Gegenbauer polynomial technique to the pion loop case to calculate the integrals involved.

We have also added the next to leading order ChPT corrections to the lowest order results and have shown that, in the corresponding energy region, results are in good agreement with predictions of other models namely, the VMD and the HLS with $a = 2$, as expected.

By investigating the momentum regions that each model predicts to have a part in the a_μ^{LbL}, we have found out why the HLS prediction for the pion loop contribution is so different with that of the VMD.

Also, using the OPE approach to the $\gamma\gamma\pi\pi$ amplitude, it has been shown that the VMD lives up to the expectation but, HLS with $a = 2$ does not and hence, the HLS can be ruled out as a valid model to consider the pion loop contribution to the muon anomalous magnetic moment. The $a = 1$ case which has a better higher energy behavior has final results similar to VMD.

Acknowledgments

References

[1] F. Jegerlehner and A. Nyffeler, Phys. Rept. **477** (2009) 1 [arXiv:0902.3360 [hep-ph]].

[2] J. P. Miller, E. de Rafael and B. L. Roberts, Rept. Prog. Phys. **70** (2007) 795 [hep-ph/0703049].

[3] M. Knecht, Lect. Notes Phys. **629** (2004) 37 [hep-ph/0307239].

[4] M. Passera, Phys. Rev. D**75** (2007) 013002 [hep-ph/0606174].

[5] S. Scherer , Adv. Nucl. Phys. **27** (2003) 277

[6] J. Bijnens and J. Prades, Mod. Phys. Lett. A **22** (2007) 767 [hep-ph/0702170 [HEP-PH]].

[7] K. Nakamura *et al.* [Particle Data Group Collaboration], J. Phys. G G **37** (2010) 075021.

[8] J. Prades, E. de Rafael and A. Vainshtein, (Advanced series on directions in high energy physics. 20) [arXiv:0901.0306 [hep-ph]].

[9] T. Kinoshita, B. Nizic and Y. Okamoto, Phys. Rev. Lett.**54** (1984) 717

[10] M. Hayakawa, T. Kinoshita and A. I. Sanda, Phys. Rev. D **54** (1996) 3137 [hep-ph/9601310].

[11] J. Bijnens, E. Pallante and J. Prades, Phys. Rev. Lett. **75** (1995) 1447 [Erratum-ibid. **75** (1995) 3781] [hep-ph/9505251].

[12] J. Bijnens, E. Pallante and J. Prades, Nucl. Phys. B **474** (1996) 379 [hep-ph/9511388].

[13] M. Hayakawa, T. Kinoshita and A. I. Sanda, Phys. Rev. Lett. **75** (1995) 790 [hep-ph/9503463].

[14] M. Knecht and A. Nyffeler, Phys. Rev. D **65** (2002) 073034 [hep-ph/0312226].

[15] J. Bijnens, E. Pallante and J. Prades, Nucl. Phys. B **626** (2002) 410 [hep-ph/0112255]; M. Hayakawa and T. Kinoshita, Phys. Rev. D **66** (2002) 019902

Erratum-ibid. D66 (2002) 019902

[16] K. Melnikov and A. Vainshtein, Phys. Rev. D **70** (2004) 113006 [hep-ph/0312226].

[17] G. W. Bennett et al., (Muon (g-2) Collaboration), Phys. Rev. D **73** (2006) 072003 [hep-ex/0602035]. Phys. Rev. D **70** (2004) 113006 [hep-ph/0312226].

[18] F. Jegerlehner Acta. Phys. Polon. B **38** (2007) 3021 [arXiv:0703125v3 [hep-ph]].

[19] S. Weinberg, Physica A **96**, (1979), 327.

[20] J. Goldstone, A. Salam and S. Weinberg, Phys. Rev. **127**, 965 (1962).

[21] J. Gasser and H. Leutwyler, Ann. Phys. (N.Y.) **158** (1985) 142, Nucl, Phys, B **250**, (1985), 465.

[22] M. Harada, K. Yamawaki, Phys. Rept. **381** (2003) 1

[23] G. Ecker, J. Gasser, A. Pich and E. de Rafael, Nucl. Phys. B **321** (1989) 311.

[24] M. Bando, T. Kugo, S. Uehara, K. Yamawaki and T. Yanagida, Phys. Rev. Lett. **54** (1985) 1215

[25] K. Engel, H. Patel, M. Ramsey-Musolf [arXiv:1201.0809v2].